

Cluster analysis of downscaled and explicitly simulated North Atlantic tropical cyclone tracks

Article

Published Version

Daloz, A. S., Camargo, S. J., Kossin, J. P., Emanuel, K., Horn, M., Jonas, J. A., Kim, D., LaRow, T., Lim, Y.-K., Patricola, C. M., Roberts, M., Scoccimarro, E., Shaevitz, D., Vidale, P. L. ORCID: <https://orcid.org/0000-0002-1800-8460>, Wang, H., Wehner, M. and Zhao, M. (2015) Cluster analysis of downscaled and explicitly simulated North Atlantic tropical cyclone tracks. *Journal of Climate*, 28 (4). pp. 1333-1361. ISSN 1520-0442 doi: <https://doi.org/10.1175/JCLI-D-13-00646.1> Available at <https://centaur.reading.ac.uk/38622/>

It is advisable to refer to the publisher's version if you intend to cite from the work. See [Guidance on citing](#).

Published version at: <http://dx.doi.org/10.1175/JCLI-D-13-00646.1>

To link to this article DOI: <http://dx.doi.org/10.1175/JCLI-D-13-00646.1>

Publisher: American Meteorological Society

All outputs in CentAUR are protected by Intellectual Property Rights law, including copyright law. Copyright and IPR is retained by the creators or other copyright holders. Terms and conditions for use of this material are defined in the [End User Agreement](#).

www.reading.ac.uk/centaur

CentAUR

Central Archive at the University of Reading

Reading's research outputs online



Cluster Analysis of Downscaled and Explicitly Simulated North Atlantic Tropical Cyclone Tracks

ANNE S. DALOZ,^a S. J. CAMARGO,^b J. P. KOSSIN,^c K. EMANUEL,^d M. HORN,^e J. A. JONAS,^f
 D. KIM,^b T. LAROW,^g Y.-K. LIM,^h C. M. PATRICOLA,ⁱ M. ROBERTS,^j E. SCOCCIMARRO,^k
 D. SHAEVITZ,^l P. L. VIDALE,^m H. WANG,ⁿ M. WEHNER,^o AND M. ZHAO^p

^a *Space Science and Engineering Center, University of Wisconsin–Madison, Madison, Wisconsin*

^b *Lamont-Doherty Earth Observatory, Columbia University, Palisades, New York*

^c *NOAA/National Climatic Data Center, Asheville, North Carolina*

^d *Massachusetts Institute of Technology, Cambridge, Massachusetts*

^e *School of Earth, University of Melbourne, Melbourne, Victoria, Australia*

^f *Center for Climate Systems, Columbia University, New York, New York, and Global Modeling and Assimilation Office, and Goddard Earth Sciences Technology and Research/I.M. Systems Group, NASA Goddard Space Flight Center, Greenbelt, Maryland*

^g *Florida State University, Tallahassee, Florida*

^h *Global Modeling and Assimilation Office, and Goddard Earth Sciences Technology and Research/I.M. Systems Group, NASA Goddard Space Flight Center, Greenbelt, Maryland*

ⁱ *Texas A&M University, College Station, Texas*

^j *Met Office Hadley Centre, Devon, United Kingdom*

^k *Istituto Nazionale di Geofisica e Vulcanologia, Bologna, and Centro Euro-Mediterraneo sui Cambiamenti Climatici, Lecce, Italy*

^l *Department of Applied Physics and Applied Mathematics, Columbia University, New York, New York*

^m *National Centre for Atmospheric Science, Department of Meteorology, University of Reading, Reading, United Kingdom*

ⁿ *NOAA/NWS/NCEP/Climate Prediction Center, College Park, and Innovim, LLC, Greenbelt, Maryland*

^o *Lawrence Berkeley National Laboratory, and University of California, Berkeley, Berkeley, California*

^p *NOAA/Geophysical Fluid Dynamics Laboratory, Princeton, New Jersey*

(Manuscript received 11 October 2013, in final form 5 November 2014)

ABSTRACT

A realistic representation of the North Atlantic tropical cyclone tracks is crucial as it allows, for example, explaining potential changes in U.S. landfalling systems. Here, the authors present a tentative study that examines the ability of recent climate models to represent North Atlantic tropical cyclone tracks. Tracks from two types of climate models are evaluated: explicit tracks are obtained from tropical cyclones simulated in regional or global climate models with moderate to high horizontal resolution (1° – 0.25°), and downscaled tracks are obtained using a downscaling technique with large-scale environmental fields from a subset of these models. For both configurations, tracks are objectively separated into four groups using a cluster technique, leading to a zonal and a meridional separation of the tracks. The meridional separation largely captures the separation between deep tropical and subtropical, hybrid or baroclinic cyclones, while the zonal separation segregates Gulf of Mexico and Cape Verde storms. The properties of the tracks' seasonality, intensity, and power dissipation index in each cluster are documented for both configurations. The authors' results show that, except for the seasonality, the downscaled tracks better capture the observed characteristics of the clusters. The authors also use three different idealized scenarios to examine the possible future changes of tropical cyclone tracks under 1) warming sea surface temperature, 2) increasing carbon dioxide, and 3) a combination of the two. The response to each scenario is highly variable depending on the simulation considered. Finally, the authors examine the role of each cluster in these future changes and find no preponderant contribution of any single cluster over the others.

Corresponding author address: Anne Sophie Daloz, Space Science and Engineering Center, University of Wisconsin–Madison, 1225 West Dayton Street, 11th floor, Madison, WI 53704.
 E-mail: adaloz@wisc.edu

DOI: 10.1175/JCLI-D-13-00646.1

1. Introduction

Tropical cyclones are one of the most devastating phenomena in the world due to their strong winds and heavy precipitation extending over wide areas (e.g., Scoccimarro et al. 2014; Villarini et al. 2014). Thus, there has been a growing demand for better understanding these phenomena and simulations of the response of tropical cyclone activity to climate change. In the past years, many studies have focused on the impact of climate change on tropical cyclone frequency and intensity (e.g., Gualdi et al. 2008; Knutson et al. 2010; Zhao and Held 2010; Stocker et al. 2014). Recently, a few studies evaluated the impact of climate change on tropical cyclone tracks over the North Atlantic basin. Murakami and Wang (2010) used a high-resolution global atmospheric model (20 km), while Colbert et al. (2013) used a beta advection model with winds from phase 3 of the Coupled Model Intercomparison Project (CMIP3); both studies showed a decrease in straight moving storm tracks reaching the Gulf of Mexico and the Caribbean Sea, as well as an increase in recurving tracks reaching the central Atlantic. These variations in tropical cyclone trajectories are very important as they are a potential cause for changes in the location of landfalling tropical cyclones.

Murakami and Wang (2010) found that these changes in tropical cyclones tracks were caused by an eastward shift in genesis location. On the other hand, Colbert et al. (2013) attributed the projected changes in tropical cyclone trajectories to the large-scale steering flow. Camargo (2013) analyzed the North Atlantic tracks in the phase 5 of the Coupled Model Intercomparison Project (CMIP5) models and obtained no robust changes in future simulations among the models. Mei et al. (2014) analyzed North Atlantic tropical cyclones track density in observations and one of the high-resolution models in this study and found that, on interannual and decadal time scales, a basinwide mode dominates, which is related to the interannual frequency in the basin. Strazzo et al. (2013) used a spatial lattice technique to analyze two of the models in this study and identified regional biases in the North Atlantic tropical cyclone activity. These studies highlighted the importance of accurately simulating the tropical cyclone tracks in addition to the frequency and intensity of tropical cyclones.

To evaluate the ability of modern climate models to represent the North Atlantic tropical cyclone tracks, the characteristics of simulated tracks are explored through the use of a cluster technique (Kossin et al. 2010). The cluster technique applied to observed tracks leads to a meridional and a zonal separation in four groups. The meridional separation largely captures the separation between deep tropical and subtropical, hybrid or baroclinic

cyclones, while the zonal partition tends to segregate Gulf of Mexico from Cape Verde systems. Figure 1 shows the separation of the historical tracks, genesis and landfall points among each of the four clusters for National Hurricane Center North Atlantic Hurricane Database (HURDAT; Jarvinen et al. 1984) for the period 1950–2013, similarly to what was shown in Kossin et al. (2010) for the 1950–2007 storms. In the four clusters, storms in clusters 1 and 2 tend to form farther north than storms from clusters 3 and 4. Storms from clusters 1 and 3 tend to form farther east than storms from clusters 1 and 4 (cf. Fig. 1). Cluster 2 storms form almost exclusively in the Gulf of Mexico and westernmost Caribbean and usually present a northward component in their tracks. Cluster 1 storms form farther east but also tend to have a pronounced northward component. Essentially all classic “Cape Verde” tropical cyclones are found in either cluster 3 or 4. Clusters 3 and 4 are both influenced by the African easterly waves coming from the West African continent. Compared to cluster 4 storms, which tend to maintain their primarily westward track until landfall, cluster 3 storms are more often “recurving.” In this study, we first want to verify that the characteristics of the observed tropical cyclone tracks [as discussed in Kossin et al. (2010) and shown in Fig. 1] are simulated by the climate models.

The climatological properties of North Atlantic tropical cyclone tracks in moderate- to high-resolution atmospheric climate models are documented in this paper and compared to the observations. The model simulations analyzed here have been produced for the U.S. Climate Variability and Predictability Research Program (CLIVAR) Hurricane Working Group by various modeling centers. An overview of the U.S. CLIVAR Hurricane Working Group objectives and results is given in Walsh et al. (2015). As far as we know, previously, only one other intercomparison project has focused on the study of tropical cyclone activity: the Tropical Cyclone Climate Model Intercomparison Project (TC-MIP; Walsh et al. 2010). However, in that project a different set of simulations was studied. Daloz et al. (2012) showed that in the TC-MIP simulations the majority of climate models have problems representing tropical cyclone activity on the eastern Atlantic because of biases in large-scale fields and/or African easterly wave activity. These issues will also be examined for some models in this study (depending on availability). Here, both explicit and downscaled North Atlantic tropical cyclone tracks are examined.

The explicit tropical cyclone tracks originated from nine climate models (global and regional) with a spatial resolution varying from 0.25° to 1° . Tracks were obtained using detection and tracking algorithms that find and track storms in the output of these climate models. Typically,

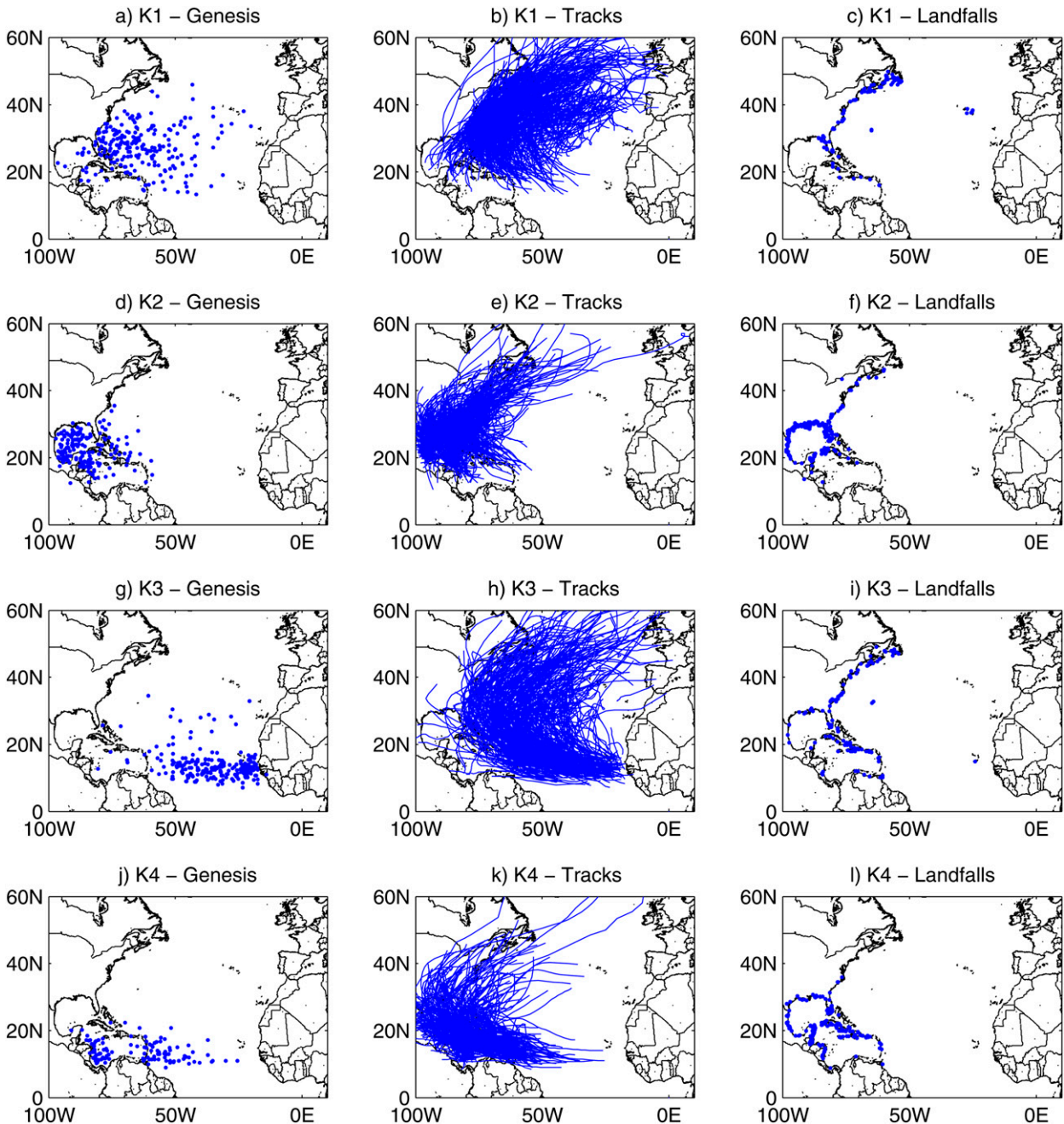


FIG. 1. Observed North Atlantic tropical cyclone tracks, genesis locations, and landfall locations during the period 1950–2013 for HURDAT, as separated by the cluster analysis. This figure is similar to what was shown in [Kossin et al. \(2010\)](#) for the period 1950–2007.

each modeling group developed their own tracking algorithm using very similar but different criteria to define and track the model storms. This is clearly a limitation of our analysis; therefore, our results should be considered tentative. This issue will be further addressed below. The tracking algorithms have specific criteria for several dynamic and thermodynamic variables leading to the detection and tracking of tropical cyclone-like systems

([Walsh 1997](#); [Camargo and Zebiak 2002](#); [Chauvin et al. 2006](#)). The climate models are forced with prescribed climatological sea surface temperatures (SSTs): that is, with the same values every year, varying monthly with the seasonal cycle for a climatological season. As the models are forced with climatological SSTs, it will not be possible to consider climate variability in our analysis. The modulation of North Atlantic tropical cyclones by El Niño–Southern

Oscillation (ENSO) in the same set of models was analyzed in Wang et al. (2014) (global climate models) and Patricola et al. (2014) (regional climate model). Here we will evaluate the ability of the different models to correctly simulate the main characteristics of North Atlantic tropical cyclones, such as track types, frequency, intensity, and duration. A description of the global characteristics of the tropical cyclones in the same set of models for the present climate was presented in Shaevitz et al. (2015).

Previous studies showed that a realistic simulation of tropical cyclones structure and intensity requires high horizontal- and vertical-resolution models (Rotunno et al. 2009; Rao et al. 2010; Zhang and Wang 2003; Manganello et al. 2012; Strachan et al. 2013; Walsh et al. 2013; Wehner et al. 2015; Zarzycki and Jablonowski 2014). Manganello et al. (2012) obtained realistic intensities as well as eyewall structure with a climate model of horizontal resolution of 0.1° . However, the horizontal resolution of most climate models ($>0.25^\circ$) is too coarse to adequately resolve these storms, especially the most intense storms. Low-resolution climate models ($\sim 2^\circ\text{--}3^\circ$) are able to produce tropical cyclone-like storms, but some of the tropical cyclone characteristics, such as size and intensity, differ from the observed ones (e.g., Camargo et al. 2005).

To deal with these high-resolution requirements, several downscaling techniques have been developed. In the second part of this paper, we analyze the results from tropical cyclones obtained with the statistical-dynamical downscaling technique described in Emanuel (2006) and Emanuel et al. (2006). One benefit of this type of downscaling technique is to generate a very large number of synthetic storm tracks with realistic intensity based on climate model environmental fields. This technique has been successfully applied to various reanalyses (Emanuel 2010) and climate models (Emanuel et al. 2008, 2010; Emanuel 2013) and coupled with storm surge models (Lin et al. 2012). However, this technique also presents some drawbacks such as the absence of statistics of potential initiating disturbances (e.g., African easterly waves). This point will be further discussed in the article. Here we compare the tracks obtained by downscaling the large-scale variables simulated by four of the climate models analyzed in the first part of the study.

Finally, simple future climate projections are examined. The independent and combined effects of an increase in CO_2 and a uniform warming of SST are considered. Previous studies with prescribed SSTs (e.g., Sugi et al. 2002; Bengtsson et al. 2007) as well as coupled models (Yoshimura and Sugi 2005; Gualdi et al. 2008; Held and Zhao 2011) showed that, at a global scale, there is a projected small decrease in the global tropical cyclone frequency in future climates [see a review in Knutson et al. (2010)]. Yoshimura and Sugi (2005) examined the impacts of increased SST and

CO_2 on tropical cyclone activity separately. The same effects were examined by Held and Zhao (2011), who found that both SST warming and CO_2 doubling have an important role in the global decrease of TC frequency in future climates. In this study, we would like to determine if the results from Held and Zhao (2011) are robust across the tropical cyclones from various climate models in the North Atlantic basin, as well as for the tropical cyclones obtained by downscaling these climate models.

Kossin et al. (2010) determined that clusters could contribute differently to the observed trends in the North Atlantic storm frequency in the current climate. They showed that trends are governed by the deep tropical storms (cluster 3), which account for most of the major tropical cyclones. This cluster is therefore very important as it contains some of the most dangerous tropical cyclones. Furthermore, several studies showed an intensification of tropical activity in future climates (Chauvin et al. 2006; Oouchi et al. 2006; Knutson et al. 2010; Villarini and Vecchi 2013). One can wonder if the potential intensification of North Atlantic tropical cyclones in the future climate could be attributed to changes in frequency or intensity of a specific cluster. This topic will be explored in the last part of our results.

In summary, the objectives of this study are (i) to examine simulated North Atlantic tropical cyclone tracks from explicit and downscaled simulations and determine if they are able to reproduce the main characteristics of the observed North Atlantic tropical cyclone clusters obtained in Kossin et al. (2010); (ii) to investigate the tropical cyclone track clusters for different models, considering different ways of generating the tropical cyclones (explicitly or downscaling) and different scenarios (climatological SST, SST warming, an increase of CO_2 , or both); and (iii) to determine if the projected changes in tropical cyclone activity over the North Atlantic basin could be attributed to specific clusters.

Section 2 summarizes the cluster technique and describes the models and the tracking algorithms used. In section 3, the characteristics of the explicitly simulated North Atlantic tropical cyclone clusters are analyzed. In section 4, the same analysis is performed for the downscaled tropical cyclones. Section 5 explores, using clusters, future changes in frequency and intensity of North Atlantic tropical cyclones. Finally, a summary and a discussion of our results are presented in section 6.

2. Clustering method and data

a. Clustering method

The cluster technique used in this study relies on a mixture of quadratic regression models, which are used

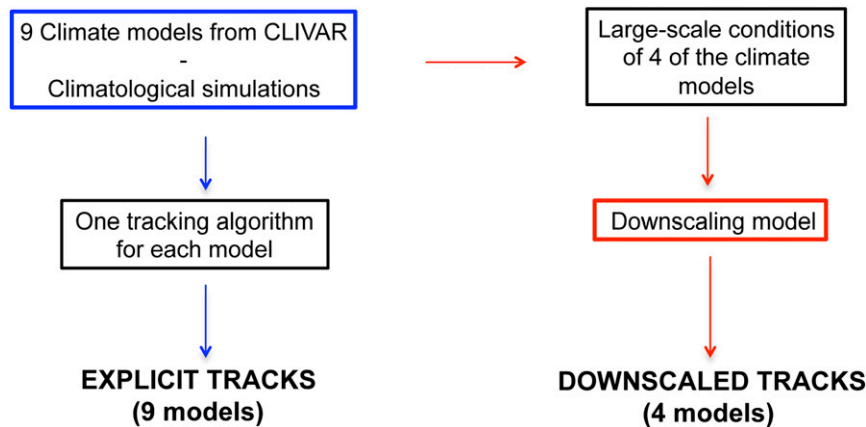


FIG. 2. Schematic representation of the explicit and downscaled simulations.

to fit the geographical shape of tropical cyclone tracks. Each component of the mixture model uses a polynomial regression curve of storm position against time. Each track is assigned to one of K different regression models. Each model is described by a set of different parameters, a regression coefficient, and a noise matrix. The cluster technique is described in detail in Gaffney et al. (2007). The technique has already been applied to observed tropical cyclone tracks in various regions, namely the North Atlantic (Kossin et al. 2010), western North Pacific (Camargo et al. 2007), eastern North Pacific (Camargo et al. 2008), Southern Hemisphere (Ramsay et al. 2012), and Fiji (Chand and Walsh 2009).

Kossin et al. (2010) showed that, for North Atlantic observed tropical cyclone tracks, the optimal number of clusters was four. In that study, an in-sample log-likelihood value narrowed down the ideal number of cluster to values between three and six clusters. The final selection, four clusters, was qualitatively based on physical characteristics of the basin. The first factor considered was the modulation of the North Atlantic tropical cyclone activity by the Atlantic meridional mode (AMM) and ENSO. Another selection factor was based on how well the clusters represented subsamples of storm tracks based on geographic location of tropical cyclogenesis. At least four clusters were necessary to correctly characterize the track types that appeared in the subsamples examined. Based on these combined factors, four clusters was the optimal choice. In this study, we also choose to use four clusters, as we wanted to compare the results of the models with those from observations. Figure 1 shows the resulting tracks, genesis and landfall locations obtained when applying this cluster technique to the observed North Atlantic tropical cyclone tracks [extending the results of Kossin et al. (2010) through 2013].

Also the analyses on the observed clusters are performed over the period from 1950 to 2013 for the observations. Landsea et al. (2010) showed that including the presatellite era tends to introduce an underestimate of the number of shorter tracks. In our case, including the presatellite era does modify the number of storms in clusters 3 and 4 but does not change the other characteristics of the clusters. The results of cluster analysis could be potentially sensitive to the track length; however, Camargo et al. (2007) showed that cluster assignments are modified because of the track length only when very drastic changes are done.

b. Explicit simulations

Two types of experiments are used in this study, namely explicit and downscaled simulations, as explained in the Introduction and shown in Fig. 2. The explicit tropical cyclones were generated from nine climate models listed in Table 1. The model simulations were forced with prescribed climatological SST and sea ice from the Hadley Centre Sea Ice and Sea Surface Temperature Experiment dataset (HadISST; Rayner et al. 2003). The radiative gas forcing follows the 1992 Intergovernmental Panel on Climate Change (IPCC) specifications. Four types of simulations are used: a control experiment and three idealized warming scenarios. The control experiment (CTL) is forced with climatological SST (climatological mean of the period 1981–2005). There are three idealized future simulations. The first future experiment corresponds to the climatological SST with 2 K added globally, “plus 2K” (p2K). The second future experiment, named “double CO₂” (2CO₂), is forced with the same climatological SST, but the CO₂ concentration is doubled in the atmosphere. In the third future experiment, “plus 2K and double CO₂” (p2K2CO₂) is the combination of the last two scenarios: that is, the models are forced with climatological SST

TABLE 1. Presentation of the explicit and downscaled simulations from CLIVAR. The models are classified going from higher to lower horizontal resolution. (Model name expansions are provided in a searchable list at <http://www.ametsoc.org/PubsAcronymList>, under the heading “Climatic, meteorological, oceanographic, and other models”.)

Model: institution	Horizontal and vertical resolutions; No. of years	Type of simulations	Name of the simulations in the article	Model description reference	Reference for the tracking methodology
CAM5.1: National Center for Atmospheric Research (NCAR), United States	0.25°, 30 levels; 65 yr	Explicit Downscaled	CAM5_E CAM5_D	Wehner et al. 2015 Emanuel et al. 2008	Knutson et al. 2007 —
WRF: Texas A&M University, United States	0.25°, 28 levels; 40 yr	Explicit–lateral boundary conditions: NCEP-2	WRF_E	Skamarock et al. 2008	Walsh 1997
HIRAM2.1: Geophysical Fluid Dynamics Laboratory (GFDL), United States	0.5°, 32 levels; 80 yr	Explicit Downscaled	GFDL_E GFDL_D	Anderson et al. 2004; Zhao et al. 2009 Emanuel et al. 2008	Zhao et al. 2009 —
GEOS5: National Aeronautics and Space Administration (NASA) Global Modeling and Assimilation Office, United States	0.5°, 72 levels; 76 yr	Explicit	GSFC_E	Rienecker et al. 2008	Vitart et al. 2003
HadGEM3A: Met Office Hadley Centre, United Kingdom	0.6°, 85 levels; 24 yr	Explicit	HG3A_E	Walters et al. 2011	Strachan et al. 2013
ECHAM5: Centro Euro- Mediterraneo per I Cambiamenti Climatici (CMCC), Istituto Nazionale di Geofisica e Vulcanologia (INGV), Italy	0.9°, 31 levels; 80 yr	Explicit Downscaled	CMCC_E CMCC_D	Roeckner et al. 2003; Scoccimarro et al. 2011 Emanuel et al. 2008	Walsh 1997 —
GISS-GCM: NASA GISS and Columbia University, United States	1°, 40 levels; 40 yr	Explicit Downscaled	GISS_E GISS_D	Schmidt et al. 2014 Emanuel et al. 2008	Camargo and Zebiak 2002 —
GFS: National Centers for Environmental Prediction (NCEP), United States	1°, 64 levels; 40 yr	Explicit	GFS_E	Saha et al. 2014	Zhao et al. 2009
FSU-GCM: Center for Ocean–Atmospheric Prediction Studies (COAPS), Florida State University, United States	1°, 27 levels; 15 yr	Explicit	FSU_E	Cocke and LaRow 2000; LaRow et al. 2008	LaRow et al. 2008

with 2 K added globally and a doubling of the CO₂ concentration.

c. Tracking algorithms

The simulated tropical cyclones were tracked by each modeling group using the tracking methodology normally adopted by them. The tracking routines used in most groups are based in very similar principles, but there are differences among them. The criteria chosen and the thresholds vary depending on the tracking algorithm and the spatial resolution for each model. The

tracking algorithms employed in this study are all described in the [appendix](#).

Previous studies showed that the frequency of tropical cyclones could be sensitive to the method of identification of the storms (Walsh et al. 2007; Horn et al. 2014). Horn et al. (2014) showed that the basic differences between tracking schemes are not of primary importance however differences in duration, wind speed, or formation-latitude thresholds are crucial. After homogenization of these thresholds, there is large agreement between different tracking schemes. The sensitivity of the cluster analysis

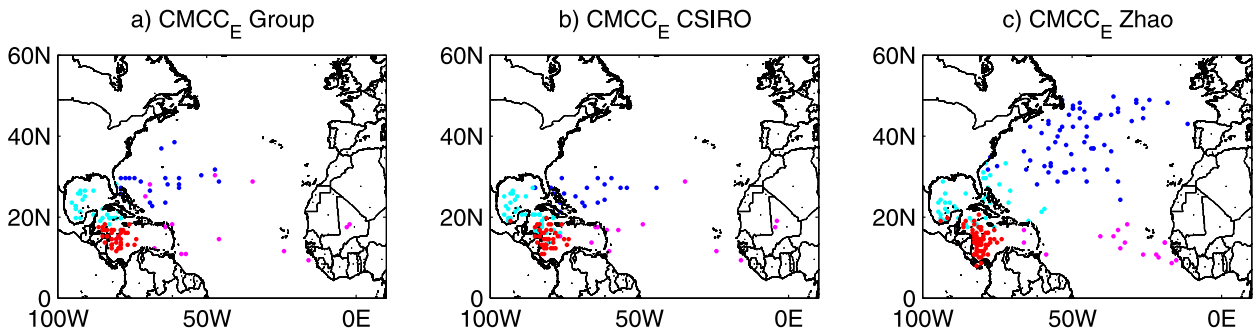


FIG. 3. North Atlantic tropical cyclone genesis locations of the tracks for CMCC_E, as separated by the cluster analysis. Tropical cyclones tracks are detected with the tracking algorithm from (a) Walsh (1997), (b) Camargo and Zebiak (2002), and (c) Zhao et al. (2009). Cluster 1 is in dark blue, cluster 2 is in light blue, cluster 3 is in pink, and cluster 4 is in red.

to the tracking techniques (described in the appendix) has been examined for two models using the data from Horn et al. (2014): only the results for the CMCC_E model (cf. Table 1) are presented here. This has to be considered as a tentative analysis, as we could not test all the models and tracking algorithms. Three different tracking algorithms were employed to detect the North Atlantic tropical cyclones tracks. The first tracking algorithm is the one originally used by the group for tracking the tropical cyclones; it follows the criteria defined in Walsh (1997). The second one is a modified Commonwealth Scientific and Industrial Research Organization (CSIRO) tracking scheme (Walsh et al. 2007; Horn et al. 2013). Finally, the third algorithm is the one from Zhao et al. (2009). The first and second tracking algorithms have similarities as they both are based on the algorithm of Walsh (1997); this should be kept in mind as we examine the results of the test.

Figure 3 presents the results of the test and shows the location of the genesis points for the four clusters using the three tracking algorithms. Here, our focus is not on the ability of CMCC_E to simulate the clusters, but to evaluate the differences among the clusters using different detection schemes. Figure 3 shows that the position of the genesis points in each cluster is very similar when using the tracking algorithms from Walsh (1997) (Fig. 3a) or Horn et al. (2013) (Fig. 3b). This is certainly due to the similarities in these two tracking algorithms, as explained above. Cluster 1 storms are developing over high latitudes, cluster 2 storms tend to appear over the Gulf of Mexico, and cluster 4 storms appear over the Caribbean Sea. Finally, cluster 3 storms develop over a band going from the Caribbean Islands to the West African coast. Some differences appear when using the tracking scheme from Zhao et al. (2009) (Fig. 3c). Clusters 2 and 4 are similar for the three tracking schemes, but some differences appear for clusters 1 and 3. The genesis points of cluster 1 are located farther north, while more

genesis points appear off the West African coast for cluster 3 storms when detected with the scheme from Zhao et al. (2009). However, these differences do not change the general characteristics of the storms in each cluster. For instance, cluster 1 storms, in all three tracking algorithms, are tropical cyclones that tend to develop over higher latitudes, while cluster 3 storms are systems that tend to develop in the eastern part of the Atlantic basin.

Complementary to Fig. 3, Table 2 presents the number of tropical cyclones detected per year for CMCC_E using the three different tracking algorithms. The number of tropical cyclones detected is the same when using the scheme from Walsh (1997) or the modified CSIRO scheme. However, when using the scheme from Zhao et al. (2009), there are differences. The total number of tropical cyclones per year increases from 1.5 to 2.4, but it does not change the main result: that is, CMCC_E highly underestimates the number of tropical cyclones over the North Atlantic basin. The differences in the number of TC mainly come from clusters 1 and 4, which double with the Zhao scheme.

In summary, while we do not think that using different tracking algorithms for comparing tropical cyclone

TABLE 2. Number of tropical cyclones per year detected with the tracking algorithms from (i) Walsh (1997), (ii) Horn et al. (2013), and (iii) Zhao et al. (2009) for each cluster and the total, for the explicit simulation CMCC_E, and (iv) for the observations (HURDAT: 1950–2013).

CMCC_E	Cluster 1	Cluster 2	Cluster 3	Cluster 4	Total
Walsh (1997)	0.3	0.5	0.2	0.5	1.5
Horn et al. (2013)	0.3	0.5	0.2	0.5	1.5
Zhao et al. (2009)	0.8	0.6	0.2	0.8	2.4
Observations	3.5	2.9	3.7	2.3	12.4

tracks is ideal, for the present study, the use of the same tracking algorithm for all the models was not possible. Therefore, we decided to use the tracks available to us, keeping in mind that differences that we find among the models can be due to the differences between the models themselves but also probably be partly attributed to the differences in tracking algorithms. Therefore, we will not specifically compare the number of tropical cyclones between each cluster for the explicit simulations but just discuss cases in which a model highly underestimates or overestimates the number of systems produced compared to the observations and other models. The use of different tracking algorithms modifies some of the characteristics of the clusters (e.g., number); however, it cannot change the ability of a model to produce tropical cyclones. The high underestimation of the number of storms of CMCC_E cannot be completely removed by a change in tracking algorithm. The difference of algorithm only slightly changes the total number of storms, especially the number of weak storms, which can be more sensitive to the specific thresholds in the different tracking algorithms. So, the comparison of some of the characteristics of the clusters between observations and different models is still pertinent.

d. Downscaled simulations

For the downscaled simulations, the technique developed by Emanuel et al. (2006) was used. The downscaled simulations are described in Fig. 2 and Table 1. The downscaling technique of Emanuel et al. (2006, 2008) consists of, first, initiating storms by random seeding in space and time with warm-core vortices that have peak wind speeds of 12 m s^{-1} . The random “seeds” are planted everywhere and at all times, regardless of latitude, sea surface temperatures, season, or other factors, except that storms are not allowed to form equatorward of 2° latitude. Then the storms are propagated forward with a beta and advection model driven by winds derived by the four climate models presented in Table 1. The seeds are not considered to form tropical cyclones unless they develop winds of at least 21 m s^{-1} . Only four downscaled simulations were performed because of a lack of data from the climate models output when the downscaled simulations were performed.

To derive the storm intensity along each track, a very high-resolution coupled atmosphere–ocean hurricane model is used: namely, the Coupled Hurricane Intensity Prediction System (CHIPS; Emanuel et al. 2006). CHIPS is an axisymmetric atmospheric model in potential radius coordinates (Schubert and Hack 1983). CHIPS is coupled to a simple, one-dimensional ocean model that captures most of the effects of upper-ocean mixing. The atmospheric model can reach a couple of

kilometers of horizontal resolution. The potential radius coordinates permit obtaining high resolution for the eye and the eyewall using a relatively small number of radial nodes. Inputs to CHIPS are in the form of monthly-mean climatological potential intensity (which combines the thermodynamic control on tropical cyclone intensity of both the sea surface temperature and the environmental atmospheric temperature profile). Ocean mixed layer depth and thermal stratification of the ocean below the mixed layer are all interpolated to the position and time of the storm. Emanuel et al. (2004) studied the effect of using monthly-mean climatological intensity instead of daily data and found that it was minimal in most cases.

Previous studies have already demonstrated that the tropical cyclone activity from this downscaling technique is generally realistic (e.g., Emanuel et al. 2006; Emanuel 2010). For instance, Emanuel et al. (2006) showed that, when driven by NCAR–NCEP reanalysis (Kalnay et al. 1996), the synthetic tracks obtained capture correctly the observed spatial and seasonal variability of tropical cyclones around the globe. However, this technique presents some drawbacks such as the lack of the feedbacks between the tropical cyclones and their environment. Also, notably absent from this technique is the statistics of potential initiating disturbances, such as African easterly waves. This may impact the realism of the timing of the development of tropical cyclones over the eastern part of the North Atlantic basin.

3. Climatology of clusters from explicit simulations

a. Tracks and genesis

Figure 4 presents the general climatology of North Atlantic tropical cyclone genesis by cluster membership for observations (Fig. 4a: HURDAT dataset period 1950–2013; Jarvinen et al. 1984) and the nine explicit simulations (Figs. 4b–j) described in Table 1. Table 3 summarizes various measures of tropical cyclone activity for each of the four clusters shown in Fig. 4 for observations and the nine models. These figures and Table 3 clearly show the separation of the North Atlantic tropical cyclone genesis (Fig. 4) locations in each of the four clusters, with meridional and zonal separations between the clusters. The separation between the clusters is examined deriving the mean position of TCs in each cluster (cf. Table 3). The number of North Atlantic tropical cyclones for most of the explicit simulations is smaller than in observations. For some models, there were only 10 or 15 tropical cyclones over the entire time period of the control simulation. To have a large sample size and to apply the same procedure for all the simulations, the cluster analysis was performed for each model using all

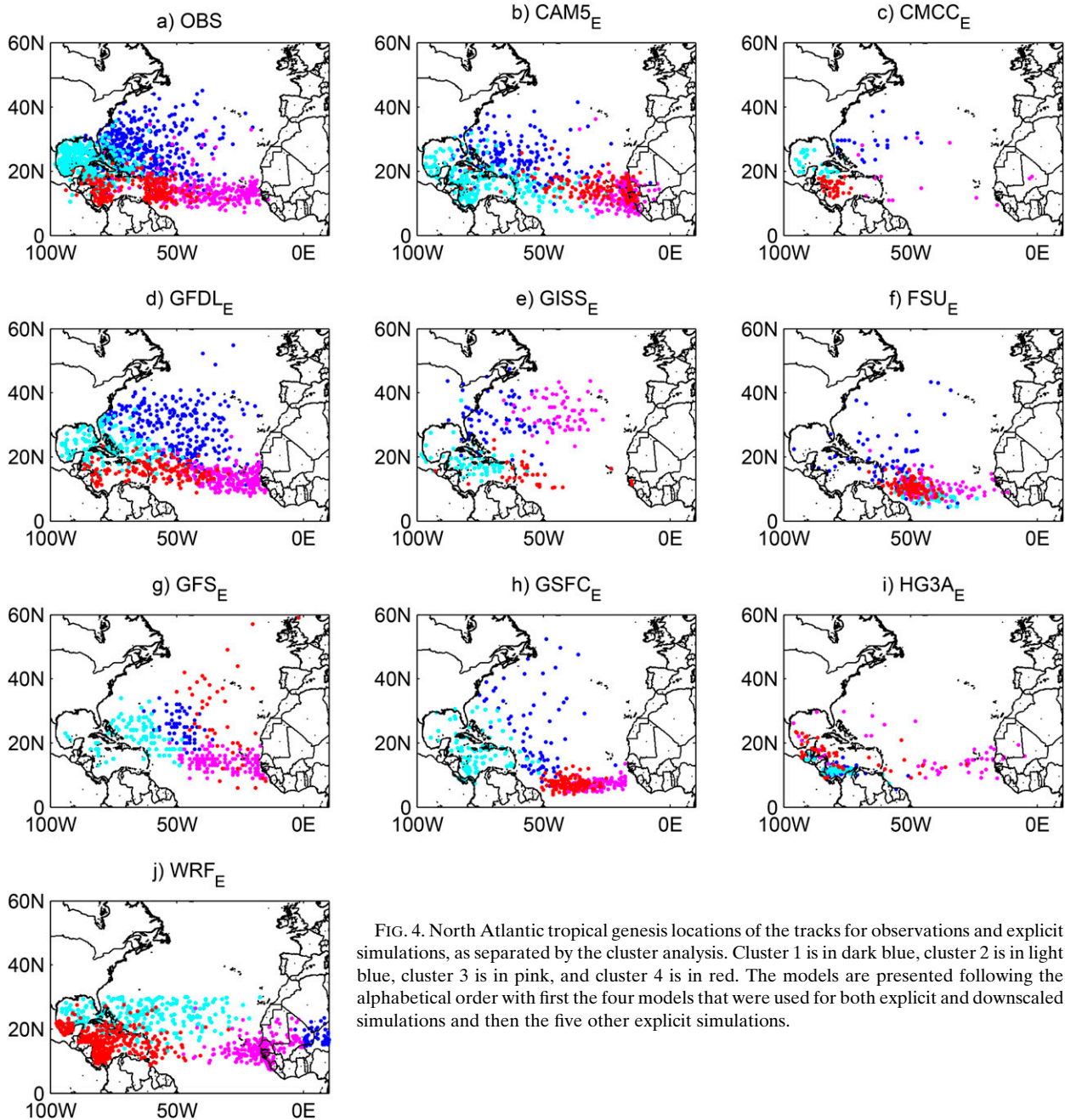


FIG. 4. North Atlantic tropical genesis locations of the tracks for observations and explicit simulations, as separated by the cluster analysis. Cluster 1 is in dark blue, cluster 2 is in light blue, cluster 3 is in pink, and cluster 4 is in red. The models are presented following the alphabetical order with first the four models that were used for both explicit and downscaled simulations and then the five other explicit simulations.

the ensembles and scenarios simultaneously. We did sensitivity tests for the model with most storms (GFDL_E) and determined that applying the cluster analysis to all the scenarios simultaneously would not lead to different results than if we applied the cluster analysis for each scenario separately (not shown). It is important to notice that the cluster analysis has no knowledge of which simulation the track belongs to. Therefore, as we wanted to use the same methodology for all models, the models with a very low number of storms restricted us to apply the

cluster analysis to all the tracks in a model together, independently of the scenario. Once the storms are classified in clusters, we examine if there are differences in the characteristics of the clusters for the different scenarios.

The comparison of the cluster analysis applied to North Atlantic tropical cyclones in observations (Fig. 4a) with the simulated tropical cyclones in GFDL_E (Fig. 4d) shows encouraging results. There is a good agreement in terms of cluster separation (Table 3) for the genesis locations (Fig. 4) between the observations and GFDL_E.

TABLE 3. Comparison of various measures by cluster for the observations from HURDAT (1950–2013) and the nine explicit simulations. Percent values (in parentheses) represent the proportions of tropical cyclones from each cluster to the total number of tropical cyclones.

All runs	Dataset	Cluster 1	Cluster 2	Cluster 3	Cluster 4	Total
No. of TC per year	OBS	3.5 (28%)	2.9 (24%)	3.7 (30%)	2.3 (18%)	12.4
	CAM5_E	2.6 (26%)	3.5 (35%)	1.7 (18%)	2.1 (21%)	9.9
	CMCC_E	0.3 (18%)	0.5 (33%)	0.2 (14%)	0.5 (35%)	1.5
	GFDL_E	3.7 (34%)	2.2 (21%)	2.8 (26%)	2.0 (19%)	12.7
	GISS_E	1.7 (28%)	1.7 (28%)	1.7 (29%)	0.9 (15%)	6.0
	FSU_E	5.5 (22%)	6.4 (24%)	6.4 (24%)	7.9 (30%)	26.2
	GFS_E	1.7 (19%)	2.1 (25%)	3.6 (42%)	1.1 (14%)	8.5
	GSFC_E	1.0 (17%)	1.5 (26%)	1.6 (29%)	1.6 (28%)	5.7
	HG3A_E	2.1 (25%)	2.3 (27%)	2.2 (26%)	1.9 (22%)	8.5
	WRF_E	1.2 (5%)	6.5 (29%)	6.2 (27%)	8.7 (39%)	22.6
Mean position (latitude, longitude)	OBS	27°N, 64°W	22°N, 84°W	14°N, 37°W	14°N, 65°W	
	CAM5_E	24°N, 59°W	17°N, 72°W	12°N, 18°W	15°N, 30°W	
	CMCC_E	29°N, 66°W	21°N, 86°W	18°N, 50°W	15°N, 80°W	
	GFDL_E	28°N, 51°W	23°N, 76°W	14°N, 29°W	15°N, 58°W	
	GISS_E	32°N, 69°W	18°N, 80°W	34°N, 44°W	15°N, 55°W	
	FSU_E	18°N, 66°W	9°N, 44°W	11°N, 40°W	10°N, 49°W	
	GFS_E	25°N, 48°W	22°N, 66°W	14°N, 31°W	28°N, 32°W	
	GSFC_E	23°N, 53°W	17°N, 76°W	7°N, 29°W	7°N, 40°W	
	HG3A_E	11°N, 78°W	12°N, 84°W	16°N, 43°W	16°N, 78°W	
	WRF_E	18°N, 20°E	24°N, 64°W	14°N, 18°W	17°N, 78°W	
Mean duration per TC (days)	OBS	6.2	5.6	10.6	8.4	
	CAM5_E	8.1	8.5	12.6	13.1	
	CMCC_E	2.1	3.3	4.0	3.6	
	GFDL_E	8.3	9.1	10.1	9.8	
	GISS_E	15.6	14.3	14.6	13.7	
	FSU_E	10.6	15.1	11.4	12.3	
	GFS_E	5.1	5.4	5.5	5.4	
	GSFC_E	3.6	3.3	3.8	3.5	
	HG3A_E	16.2	16.6	15.6	11.4	
	WRF_E	4.8	4.3	6.8	5.0	
Mean LMI per TC (m s^{-1})	OBS	34	34	43	44	
	CAM5_E	46	48	42	58	
	CMCC_E	21	22	23	22	
	GFDL_E	44	45	42	43	
	GISS_E	16	14	17	12	
	FSU_E	34	37	35	38	
	GFS_E	22	21	22	24	
	GSFC_E	20	17	16	16	
	HG3A_E	23	26	32	26	
	WRF_E	29	37	34	39	
Mean PDI per TC ($10^{10} \text{ m}^3 \text{ s}^{-2}$)	OBS	1.2	1.0	4.0	2.8	
	CAM5_E	3.5	3.6	4.9	8.8	
	CMCC_E	0.1	0.2	0.3	0.2	
	GFDL_E	3.3	3.5	4.6	3.9	
	GISS_E	0.2	0.1	0.2	0.1	
	FSU_E	1.4	2.5	1.6	2.3	
	GFS_E	0.2	0.3	0.4	0.3	
	GSFC_E	0.1	0.1	0.1	0.1	
	HG3A_E	0.4	0.8	1.4	0.6	
	WRF_E	0.9	1.2	1.8	1.8	

The left panels of Fig. 5 show the tracks in each four clusters for GFDL_E. Compared to observations in Fig. 1, GFDL_E shows a good representation of the tracks (Figs. 5a,c,e,g) and landfall (not shown) locations. Figures 4a and 4d show that, for both the observations

and this explicit simulation in clusters 1 and 2, tropical cyclones tend to form farther north than in clusters 3 and 4, while the tropical cyclones in clusters 1 and 3 tend to form farther east than in clusters 2 and 4. In cluster 2, tropical cyclones tend to form almost exclusively in the

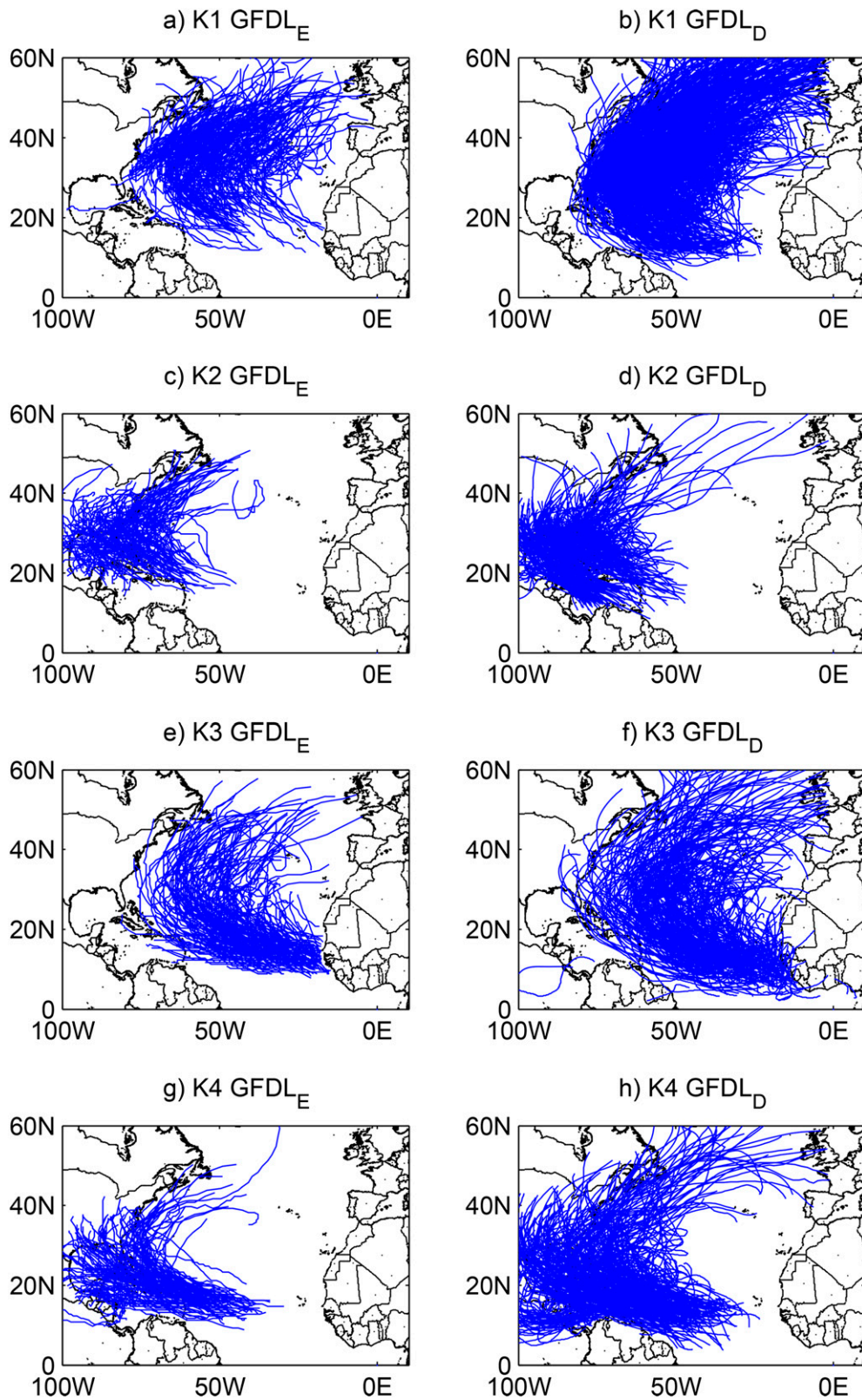


FIG. 5. North Atlantic tropical cyclone tracks for (left) GFDL_E and (right) GFDL_D, as separated by cluster analysis.

Gulf of Mexico and westernmost Caribbean, while in cluster 1 they tend to form farther east. Clusters 1 and 2 present a pronounced northward component in their tracks (Figs. 1 and 5). Essentially all classic “Cape Verde tropical cyclones” are found in clusters 3 and 4. Cluster 4 tropical cyclones tend to maintain their primarily westward track until landfall (straight movers; Figs. 1 and 5). Cluster 3 storms are more likely to “recurve” (Figs. 1 and 5), which characterizes the evolution of a storm track from westward and northward to eastward and northward (e.g., Hodanish and Gray 1993). More details about the observed clusters characteristics can be found in Kossin et al. (2010).

Unfortunately, the other models present substantial differences in their position of tropical cyclone genesis (Figs. 4b–j and Table 3) when compared to the observations (Fig. 4a). As an example, the left panels of Fig. 6 present the resulting tracks for the four clusters of GISS_E. The large disparity in the representation of tropical cyclone activity among the models can be due to several reasons, such as differences in physical parameterizations, especially convection schemes (e.g., Kim et al. 2012; Zhao et al. 2012), vertical or horizontal resolutions (Rotunno et al. 2009; Rao et al. 2010; Zhang and Wang 2003; Manganello et al. 2012; Walsh et al. 2013), and dynamical cores (Reed and Jablonowski 2011a,b, 2012). Half of the models examined here have a horizontal resolution around 1° (HG3A_E, CMCC_E, GISS_E, GFS_E, and FSU_E); however, as an accurate simulation of tropical cyclones requires high-resolution models (e.g., Rotunno et al. 2009; Manganello et al. 2012; Walsh et al. 2013), 1° is still too coarse to represent adequately many characteristics of tropical cyclones, especially intensity. However, the spatial resolution is not the only explanation for the model biases. WRF_E has the highest resolution among the models, but in WRF_E cluster 1 the tropical cyclones have an unrealistic genesis location (Fig. 4j) over the West African continent. In this case, this bias is probably coming from the tracking algorithm, which starts tracking the storms while they are still easterly waves over the West African continent.

Daloz et al. (2012) showed that many climate models present large biases when simulating tropical cyclone activity over the eastern Atlantic (clusters 3 and 4 storms). They mainly attributed these model biases to differences in large-scale fields and/or difficulties in simulating the African easterly waves over the West African coast. To further explore this hypothesis, Table 4 presents the mean African easterly wave activity over the West African continent for a subset of explicit simulations and the reanalysis ERA-Interim (1979–98; Dee et al. 2011). The African easterly wave activity was obtained using the technique from Fyfe (1999). A maximum of variance of

the 2–6-day filtered meridional wind at 850 hPa over western Africa is defined as a maximum in African easterly waves activity.

Table 4 also present the mean vertical wind shear defined as the 24-h averaged vector difference between 200 and 850 hPa over the east Atlantic basin for the same subset of explicit simulations. High values of vertical wind shear are known to be an unfavorable environment for the formation of tropical cyclones (Gray 1968). Values of vertical wind shear over around 10 m s^{-1} are detrimental to tropical cyclone development. Unfortunately, these variables could not be calculated for all the models, as the necessary data were not available. GISS_E (Fig. 4e) generates very few or misplaces cluster 3 tropical cyclones. The genesis locations for their cluster 3 cyclones are in the center of the North Atlantic basin around 40°N , while in observations genesis occurs near the West African coast around 20°N . In agreement with Daloz et al. (2012), GISS_E highly underestimates African easterly wave activity compared to ERA-Interim (cf. Table 4). On the other hand, CMCC_E (Fig. 4c) presents a reasonable African easterly wave activity but does not develop many tropical cyclones in the eastern Atlantic. Also, Bain et al. (2014) showed that the Met Office model (HG3A_E) is able to represent African easterly wave features at the climate time scale; however, it underestimates the strength and the frequency of the wave. This could partly explain the low tropical cyclone activity on the eastern part of the Atlantic basin (Fig. 4i). The unfavorable values of vertical wind shear (cf. Table 4) help explain why the genesis is concentrated in the western part of the Atlantic. It also interesting to note that, for GFS_E (Fig. 4g), most of the tropical cyclone genesis is located in the eastern part of the Atlantic basin. Furthermore, this model presents a very high-level African easterly wave activity, nearly triple what is observed in ERA-Interim, which could be associated with low values of vertical wind shear. Humidity fields would also have been a good indicator for explaining some of the differences among the models, but they were not available at the same pressure level for all the models.

b. Storm characteristics

In observations (HURDAT), the annual-mean number of North Atlantic tropical cyclones is 12.4 (tropical storms and hurricanes: i.e., named storms) for the period 1950–2013 while in the models’ explicit simulations this number varies from 26.2 and 22.6 tropical cyclones per year in the FSU_E and WRF_E models, respectively, to 1.5 tropical cyclones per year for the CMCC_E model. CAM5_E, HG3A_E, GFDL_E, and GFS_E have the most realistic values, with approximately 10 tropical cyclones per year, while GSFC_E and GISS_E have

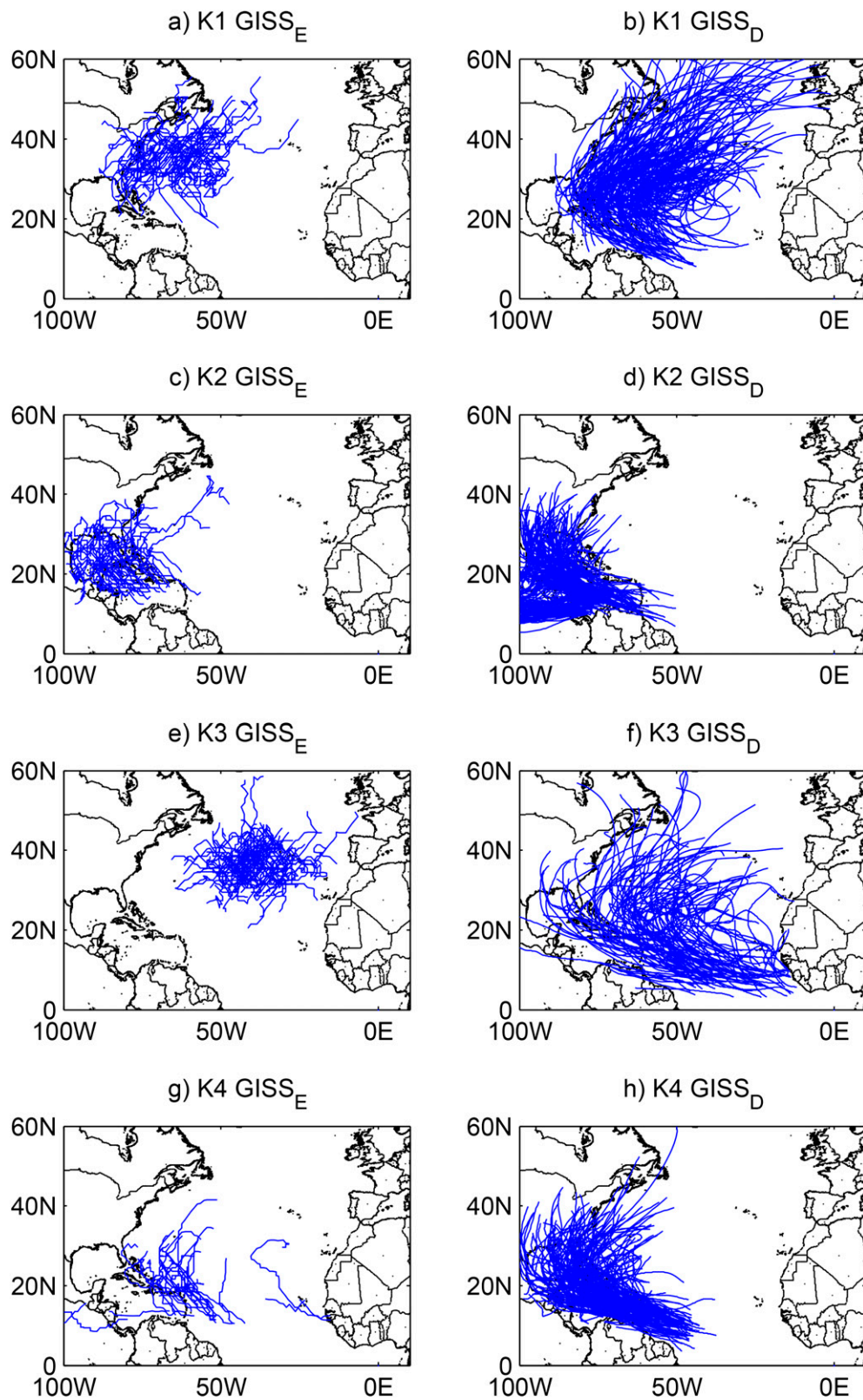
FIG. 6. As in Fig. 5, but for GISS_E and GISS_D.

TABLE 4. African easterly wave activity averaged over the West African continent (10° – 20° N, 15° W– 0°) and vertical wind shear averaged over the east Atlantic basin (10° – 20° N, 5° – 15° W) for a subset of explicit simulations and ERA-Interim only for the African easterly wave activity. The calculations were realized over the time period of each CTL runs.

Models	African easterly wave activity ($\text{m}^2 \text{s}^{-2}$)	Vertical wind shear (m s^{-1})
CMCC	7.7	12.0
GFS	19.7	7.9
GISS	0.4	11.5
ERA-Interim	7.3	

only around 6 tropical cyclones per year. In observations, more than half of the tropical cyclones (52%) are members of clusters 1 and 2, which form over higher latitudes (north of 20° N) and will be called here the northernmost tropical cyclones. In contrast, tropical cyclones in clusters 3 and 4 typically have genesis locations in the deep tropics (south of 20° N) and will be called here the southernmost tropical cyclones. As explained in section 2, the number of tropical cyclones per year in Table 3 is only indicative and will not be discussed because of the differences in tracking methodology. Just for confirming the difficulty of analyzing this value, for most of the explicit models, the standard deviation for the mean number of tropical cyclones per year was high, showing a large variation around the mean.

In observations (cf. Table 3), the northernmost tropical cyclones have a mean lifetime of 6.2 and 5.6 days, while the southernmost tropical cyclones mean lifetimes are longer with 10.6 and 8.4 days as they have more time to travel over the Atlantic Ocean before touching the coasts. Tropical cyclones for most of the explicit simulations have very similar mean lifetime duration for all clusters. Also, the simulated mean duration of tropical cyclones is usually different from the observations, with the northernmost tropical cyclone lifetime varying from 2.1 days for CMCC_E to 16.6 days for HG3A_E. In the case of the southernmost tropical cyclones, the mean lifetime varies from 3.5 days for GSFC_E to 15.6 days for HG3A_E. The comparison of mean duration per tropical cyclone is complicated by the fact that the models do not share the same tracking algorithms and the storm duration is highly dependent on the tracking algorithm thresholds. To examine the sensitivity of the storm lifetime to the tracking thresholds, we applied a wind criterion, which depends on the spatial resolution of the model, following Walsh et al. (2007). For seven of the nine models, our results for lifetime remain basically the same. Therefore, the lifetimes per tropical cyclone are comparable among most models, with exception of GISS_E and GSFC_E, which did not meet the criteria

because of the weak wind speeds of their storms (cf. Table 3).

Table 3 also presents a crucial variable for studying tropical cyclones, the lifetime maximum intensity. In observations, the lifetime maximum intensity (LMI; Elsner et al. 2008) has bimodal characteristics. For deriving the LMI, we used the 10-m wind speed or surface wind speed depending on the availability of the data.¹ The bimodal distribution arises from differences in LMI and lifetime duration between the northernmost and southernmost tropical cyclones. The southernmost tropical cyclones tend to reach higher intensities, because they stay longer over warm tropical waters with climatologically low vertical wind shear (Kossin et al. 2010). The first peak in LMI appears for the northernmost tropical cyclones, which achieve an average of 34 m s^{-1} associated with shorter tracks and colder SSTs. The second peak appears for the southernmost tropical cyclones, which reach a higher LMI with a mean intensity of 44 m s^{-1} , associated with longer tracks and warmer SSTs. The explicit tropical cyclone simulations do not simulate the bimodality of LMI of the northernmost and southernmost tropical cyclones, the mean LMI is nearly the same for all clusters and all the simulations. Furthermore, the intensity of the tropical cyclones is underestimated by most the models (CMCC_E, GISS_E, FSU_E, GFS_E, GSFC_E, HG3A, and WRF_E). This is a common bias of climate models (e.g., Yoshimura et al. 2006; Knutson et al. 2007; LaRow et al. 2008; Walsh et al. 2013), because of low model horizontal resolution and convective parameterization. Even WRF_E (Table 3), with the highest resolution (around 0.25°), has a mean LMI weaker than the observed LMI despite realistic peak intensities. The two other models (CAM5_E and GFDL_E) tend to overestimate the LMI, which could be due to their higher horizontal resolution.

The destruction that tropical cyclones can potentially cause can be estimated with a power dissipation index (PDI; Emanuel 2005). This index combines the frequency, duration, and intensity of the tropical cyclones. The PDI is defined as the integral of the cube of the maximum wind speed of the tropical cyclone over the period considered. Table 3 presents the mean PDI per tropical cyclone for each cluster. In the observations, the mean PDI per tropical cyclone is higher for the southernmost tropical cyclones with $4.0 \times 10^{10} \text{ m}^3 \text{ s}^{-2}$ for cluster 3 and $2.8 \times 10^{10} \text{ m}^3 \text{ s}^{-2}$ for cluster 4, while for clusters 1 and 2 it is approximately $1.0 \times 10^{10} \text{ m}^3 \text{ s}^{-2}$. Cluster 3 has the highest PDI per tropical cyclone,

¹ Each center has its own technique for deriving these quantities, which could potentially lead to small differences in LMI.

because of the higher intensity and duration of tropical cyclones in this cluster. None of the explicit simulations replicates this preponderant role of the southernmost or cluster 3 tropical cyclones, which is consistent with the previous biases encountered in terms of intensity and duration (Table 3). The mean PDI per tropical cyclone, for all clusters, is underestimated by a large amount of explicit simulations (CMCC_E, GISS_E, FSU_E, GFS_E, GSFC_E, HG3A_E, and WRF_E). Their mean PDI goes from $0.1 \times 10^{10} \text{ m}^3 \text{ s}^{-2}$ for GSFC_E and CMCC_E to $2.5 \times 10^{10} \text{ m}^3 \text{ s}^{-2}$ for FSU_E (Table 3), because of the low intensity of these model tropical cyclones. For the other models (CAM5_E and GFDL_E), the mean PDI is overestimated compared to the observed values and goes from $3.3 \times 10^{10} \text{ m}^3 \text{ s}^{-2}$ for GFDL_E to $8.8 \times 10^{10} \text{ m}^3 \text{ s}^{-2}$ for CAM5_E because of an overestimate both in intensity and mean duration of the simulated tropical cyclones.

c. Seasonality

The seasonality of cluster membership is presented in Fig. 7 for the observations and the explicit simulations. For observations (Fig. 7a), tropical cyclones of clusters 1 and 2 are prevalent during the early part of the North Atlantic tropical cyclone season (May–July). During this period, the environmental conditions are more favorable for their formation. During this period, thermodynamic conditions are usually not favorable in the tropics but higher-latitude conditions are good for baroclinic initiation of storms (McTaggart-Cowan et al. 2008). For cluster 2 storms, the scenario is different: midlatitude frontal systems can often deviate southward into the Gulf of Mexico and provide the baroclinic conditions that are favorable for cyclogenesis (Bracken and Bosart 2000). Cluster 3 tropical cyclones are mainly observed during the peak hurricane season (August–September), because of their strong modulation by African easterly waves (Landsea 1993), which peak at the same time of the seasonal cycle. During the late season (October–December), tropical cyclones from cluster 1 are predominant, because during those months environmental conditions are more favorable for the development of higher-latitude tropical cyclones. Cluster 4 storms present a broader seasonal cycle distribution with no peak in contribution along the season.

Error bars in Fig. 7 provide an indication of the differences between the simulations. The large error bars indicate that the models are presenting very different results from the observations and among them. Only three models have tropical cyclones with a similar seasonality as in observations, GFDL_E (Fig. 7d), GISS_E (Fig. 7e), and HG3A_E (Fig. 7i). For these models, the early and late seasons are well simulated with the predominance of clusters 1 and 2. However, in midseason

the peak of simulated cluster 3 tropical cyclones is underestimated, with most of the cluster 3 tropical cyclones distributed throughout the tropical cyclone season. This is a recurrent bias of the explicit simulations (cf. Fig. 7). This is probably due to biases in the simulation of the African easterly wave activity, because tropical cyclones from this cluster are very much influenced by the ability of models to simulate African easterly wave activity (Kossin et al. 2010). Moreover, many models are not able to reproduce the early and late season peaks from clusters 1 and 2. For some models, this is due to a bias in the proportion of tropical cyclones in a cluster. For example, WRF_E (Fig. 7j) largely underestimates the number of cluster 1 tropical cyclones, so it cannot simulate correctly the preponderance of this cluster in the early and late seasons. This is due to a criterion in the tracking algorithm: they do not take into account the storms developing over 30°N . GFS_E (Fig. 7g) overestimates the proportion of cluster 3 tropical cyclones, which leads to an unrealistic preponderance of cluster 3 tropical cyclones in the whole season. The bias in early and late seasons could also come from a misrepresentation of the seasonality of large-scale variables. The seasonality of clusters 1 and 2 is very much influenced by the environmental conditions, as mentioned above. Therefore, favorable conditions for cyclogenesis of the northernmost tropical cyclones might not be happening at the same time in observations and simulations. Furthermore, the large error bars in Fig. 7 put in evidence the difficulties of the explicit simulations to represent the seasonal cycle of cluster memberships, indicating the large spread among the models.

This section shows that the North Atlantic tropical cyclones in the explicit high-resolution climate model simulations present interesting results concerning cluster separation, with some models having biases, for the northernmost and/or southernmost tropical cyclones. Many models underestimate crucial variables such as the tropical cyclone intensity or PDI. Furthermore, none of the models is able to simulate the strong differences between the characteristics of the northernmost and southernmost tropical cyclones or the importance of cluster 3 tropical cyclones. In the next section, we will investigate and determine if the downscaled tropical cyclones have the same characteristics and biases as the explicitly simulated storms.

4. Climatology of clusters from downscaled simulations

a. Tracks and genesis

Figure 8 presents the general climatology of the observations and the downscaled North Atlantic tropical cyclone genesis by cluster membership (cf. Table 1). In

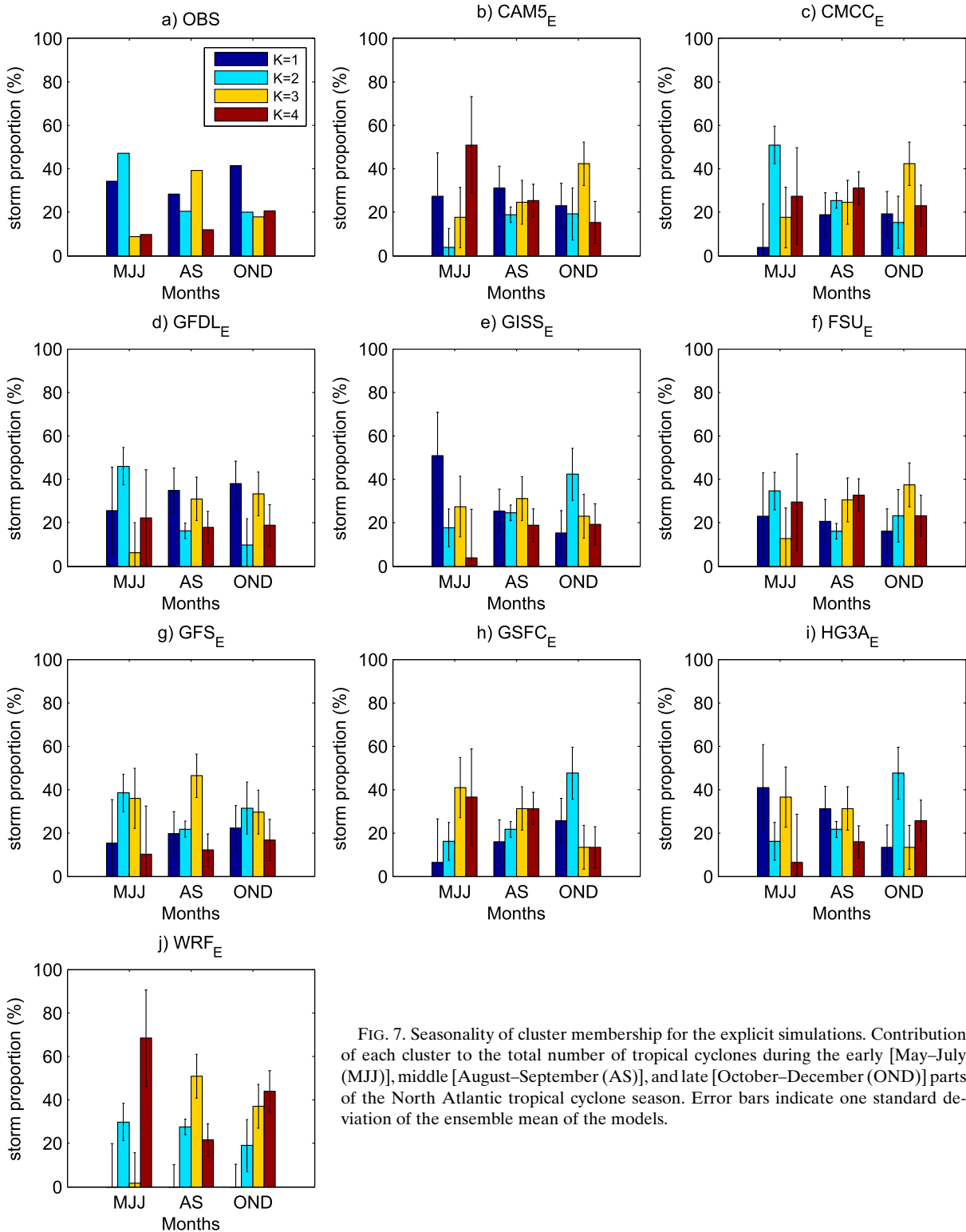


FIG. 7. Seasonality of cluster membership for the explicit simulations. Contribution of each cluster to the total number of tropical cyclones during the early [May–July (MJJ)], middle [August–September (AS)], and late [October–December (OND)] parts of the North Atlantic tropical cyclone season. Error bars indicate one standard deviation of the ensemble mean of the models.

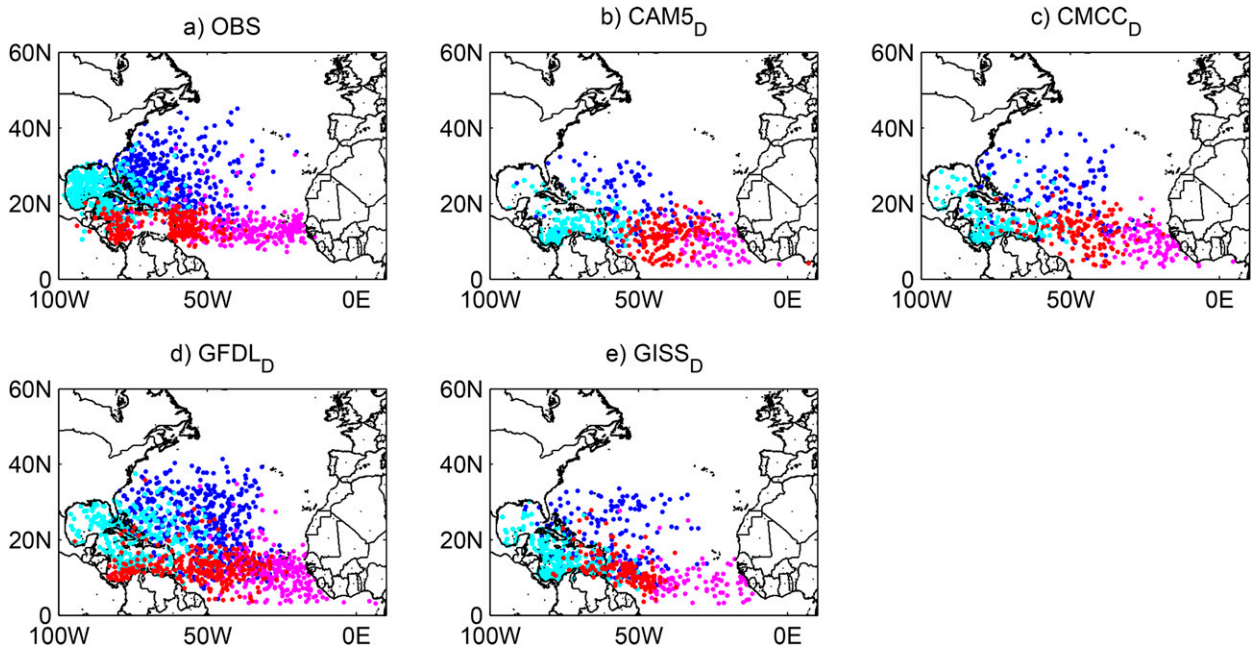


FIG. 8. As in Fig. 4, but for the downscaled simulations.

contrast to the explicit simulations (cf. Fig. 4), here only the tropical cyclones in the control run (cf. section 2) are shown, because the number of tropical cyclones generated by the downscaling methodology is very large. Over the North Atlantic basin, the number of tropical cyclones in downscaled simulations is from 2 to 6 times the number of observed tropical cyclones. It should be noted that, except for the large-scale fields, which come for the climate models, the parameters used in the downscaled simulations are the same for all cases. The differences between the simulations are therefore related to the differences in large-scale fields. It should also be mentioned that the comparison between explicit and downscaled simulations is not completely fair because of some limitations in the detections of tropical cyclones in the explicit simulations, as discussed in section 2. Also, the downscaling technique is applied to four models while the tracking techniques are applied to a single model each time.

The comparison of observations (Figs. a) with the downscaled simulations (Figs. 8b–e) reveals promising results. Also, Table 5 summarizes various measures of tropical cyclone activity for the four downscaled clusters shown in Fig. 8. There is a good agreement between the observed and simulated cluster separation in terms of genesis locations (Fig. 8 and Table 5) as well as tracks (right panels of Figs. 5 and 6) and landfall locations (not shown). It is interesting to note from Figs. 5 and 6 that explicit simulations with very different representation of the tracks can give, at a first sight at least, very similar

tracks in a downscaled configuration. To avoid redundancy, because the characteristics of the simulated clusters are very similar to the observed and these were described in the previous section, they will not be repeated here. The more realistic characteristics of the downscaled simulations are interesting, it seems that the downscaling technique manages to overcome certain biases of the model tropical cyclones analyzed the explicit simulations. For example, while CMCC_E (Fig. 4c) and GISS_E (Fig. 4e) cluster 3 tropical cyclones have a bias in genesis positions, CMCC_D (Fig. 8c) and GISS_D (Fig. 8e) manage to simulate realistically this type of tropical cyclones when compared with observations (Fig. 1). Some of the differences between the explicit and downscaled simulations could be due to the tracking technique employed but also the fact that the downscaled model generates precursors (seeds) that are not present in the explicit simulations. In the case of GISS_E, the low level of African easterly wave activity (cf. Table 3) does not provide precursors for tropical cyclone activity in the eastern part of the Atlantic. The random seeding of the downscaling technique is probably compensating for this bias.

b. Storm characteristics

For each of the simulations, 8000 synthetic tropical cyclones were generated over the globe. From these 8000 systems, the number of tropical cyclones that develop over the North Atlantic basin varies greatly among the models with 1315 systems for GFDL_D, 665 systems for GISS_D, 544 systems for CMCC_D, and 526

TABLE 5. As in Table 3, but for the downscaled simulations for the control run. Percent values (in parentheses) represent the proportions, within each cluster, of total tropical cyclone counts that reached a given intensity at some points of its lifetime or made landfall at least once.

CTL	Dataset	Cluster 1	Cluster 2	Cluster 3	Cluster 4	Total
No. of TC per year	OBS	3.5 (28%)	2.9 (24%)	3.7 (30%)	2.3 (18%)	12.4
	CAM5_D	6.8 (24%)	8.0 (28%)	5.5 (19%)	8.4 (29%)	28.7
	CMCC_D	14.4 (27%)	15.8 (29%)	10.5 (20%)	12.8 (24%)	53.5
	GFDL_D	24.8 (38%)	14.8 (22%)	12.1 (18%)	14.2 (22%)	65.9
	GISS_D	8.5 (26%)	12.0 (37%)	4.7 (14%)	7.6 (23%)	32.8
No. of major hurricane per year	OBS	0.3 (9%)	0.4 (11%)	1.3 (39%)	0.7 (41%)	2.7
	CAM5_D	0.3 (6%)	0.8 (11%)	0.7 (15%)	1.7 (22%)	3.5
	CMCC_D	1.0 (13%)	0.7 (10%)	0.9 (17%)	0.5 (8%)	3.1
	GFDL_D	5.3 (21%)	1.1 (7%)	4.4 (37%)	3.8 (27%)	14.6
	GISS_D	0.9 (11%)	1.4 (12%)	1.0 (21%)	2.5 (33%)	5.8
Mean position (latitude, longitude)	OBS	27°N, 64°W	22°N, 84°W	14°N, 37°W	14°N, 65°W	
	CAM5_D	19°N, 54°W	14°N, 71°W	10°N, 26°W	11°N, 44°W	
	CMCC_D	23°N, 56°W	15°N, 74°W	10°N, 27°W	13°N, 46°W	
	GFDL_D	23°N, 51°W	20°N, 73°W	12°N, 31°W	13°N, 54°W	
	GISS_D	21°N, 56°W	15°N, 74°W	9°N, 32°W	13°N, 46°W	
Mean duration per TC (days)	OBS	6.2	5.6	10.6	8.4	
	CAM5_D	8.0	7.4	11.3	10.3	
	CMCC_D	8.3	7.3	13.6	9.9	
	GFDL_D	8.9	6.4	12.3	10.6	
	GISS_D	8.7	8.0	13.5	9.5	
Mean LMI per TC (m s^{-1})	OBS	34	34	43	44	
	CAM5_D	34	33	36	39	
	CMCC_D	39	33	38	34	
	GFDL_D	41	31	42	41	
	GISS_D	37	34	40	42	
Mean PDI per TC ($10^{10} \text{ m}^3 \text{ s}^{-2}$)	OBS	1.2	1.1	4.0	2.8	
	CAM5_D	1.2	1.1	2.2	2.7	
	CMCC_D	1.6	1.0	3.1	1.5	
	GFDL_D	2.2	0.9	3.7	2.9	
	GISS_D	1.6	1.3	3.1	2.6	
Total PDI ($10^{10} \text{ m}^3 \text{ s}^{-2}$)	OBS	271	177	850	314	
	CAM5_D	143	173	221	420	
	CMCC_D	243	152	314	203	
	GFDL_D	1104	266	886	839	
	GISS_D	291	314	296	292	
Landfalling TC count per year	OBS	1.2 (34%)	2.6 (93%)	1.1 (33%)	1.5 (88%)	
	CAM5_D	2.2 (38%)	7.6 (99%)	1.3 (26%)	6.3 (81%)	
	CMCC_D	3.7 (50%)	7.8 (99%)	1.8 (36%)	5.7 (84%)	
	GFDL_D	10.2 (41%)	14 (95%)	4.6 (39%)	13.1 (92%)	
	GISS_D	4.2 (48%)	12.0 (99%)	2.3 (49%)	7.1 (95%)	
Mean intensity at landfall (m s^{-1})	OBS	23	25	32	31	
	CAM5_D	27	24	28	31	
	CMCC_D	31	25	32	27	
	GFDL_D	32	26	33	32	
	GISS_D	28	25	34	32	

systems for CAM5_D. This disparity in the number of storm is coming from the differences in models' large-scale environmental conditions, which were used in the downscaled simulations, with some environmental conditions being more favorable to tropical cyclogenesis in the Atlantic than others. For both the explicit and downscaled simulations, GFDL has the largest number of tropical cyclones, certainly because of favorable large-scale conditions.

Table 5 also shows the percentage of tropical cyclones in each cluster for observations and the four downscaled models. The standard deviation of the mean number of tropical cyclones per year was derived for each cluster and each simulation (not shown). Except for cluster 1 storms of CAM5_D, the results showed a lower deviation from the mean in the downscaled simulation compared to the explicit ones. This allowed us to do some preliminary analysis in the proportions of the

northernmost versus the southernmost tropical cyclones. The difference in standard deviation between the explicit and downscaled simulations certainly comes from the large number of tropical cyclones in downscaled simulations, which provides a robust sample for our analysis. The observed slightly higher percentage of the northernmost tropical cyclones (52%) compared to the southernmost tropical cyclones is also present in the four downscaled models, with differences in the percentages: 63% for GISS_D, 60% for GFDL_D, 56% for CMCC_D, and 52% for CAM5_D. However, most of the downscaled models overestimate the proportion of tropical cyclones in clusters 2 and 4 and underestimate the proportion of tropical cyclones in clusters 1 and 3. The effect of this bias will be discussed below.

A clear advantage of the downscaled simulations is that they are able to produce a realistic proportion of hurricanes (not shown here) and major hurricanes (Table 5). In the observations the number of tropical cyclones that become major hurricanes (Saffir–Simpson categories 3–5) is substantially weighted toward the southernmost systems (Table 5), with approximately 40% of tropical cyclones in clusters 3 and 4 becoming major hurricanes, while only 12% of storms in clusters 1 and 2 reach those categories. Three of the four downscaled models have a fairly realistic percentage of tropical cyclones intensifying into major hurricanes (CAM5_D, GFDL_D, and GISS_D), and these models simulate a higher rate of intensification for the southernmost tropical cyclones. However, for these models, the difference between the northernmost and southernmost tropical cyclone intensification rates is not as high as in observations. For example, in the case of GFDL_D, 37% and 27% of storms in clusters 3 and 4, respectively, reach major hurricane intensity, in contrast with 21% and 7% of storms in clusters 1 and 2, respectively (Table 5). For models CAM5_D and GISS_D, the rate of tropical cyclones that reach major hurricane intensity is highly underestimated, and there is a much weaker contrast between the northernmost and southernmost tropical cyclone intensification rates. CMCC_D has reasonable rate of storms reaching major hurricane intensity but has a similar percentage of major hurricanes among the four clusters, therefore underestimating the percentage in all clusters (10%–17%; see Table 5).

In observations, the majority of category 5 hurricanes occur in clusters 3 and 4 (Kossin et al. 2010). This is also the case for GFDL_D and GISS_D. Of the 39 (12) category 5 hurricanes that have been simulated by GFDL_D (GISS_D), 32 (8) are in clusters 3 and 4. The number of category 5 hurricanes simulated in the other two models is too low to be analyzed here.

In observations and downscaled simulations, the southernmost tropical cyclones are less frequent but have a longer lifetime than the northernmost ones (Table 5). For the downscaled simulations, the mean lifetime varies between 6.4 and 8.9 days for the northernmost tropical cyclones and between 9.5 to 13.6 days for the southernmost tropical cyclones. However, while the downscaled simulations capture the meridional difference in lifetime among the clusters, they overestimate the mean lifetime duration of all tropical cyclones. This may be partly because the downscaling technique does include the early stages of extratropical transition but does not reclassify the storms as extratropical.

As mentioned above, in observations the LMI follows a bimodal distribution with a higher mean intensity for the southernmost tropical cyclones than in the northernmost ones. All the downscaled models, with exception of CMCC_D, manage to reproduce this characteristic. CAM5_D, GFDL_D, and GISS_D have a mean LMI for the northernmost tropical cyclones between 34 and 36 ms^{-1} , while for the southernmost cyclones it varies between 38 and 42 ms^{-1} . Even if there is a more pronounced contrast in the observations, the downscaled models are able to simulate the differences in intensity between the northernmost and southernmost tropical cyclones, which is a very encouraging result.

Table 5 presents the mean PDI per tropical cyclone for each cluster. In observations, the mean PDI is clearly higher for the southernmost tropical cyclones (clusters 3 and 4) compared with the northernmost ones (clusters 1 and 2). All the downscaled models also reproduce this difference (Table 5). However, the downscaled models tend to underestimate the mean PDI of the southernmost tropical cyclones. Although in the simulations, the mean PDI varies between 2.2×10^{10} (CAM5_D) and $3.7 \times 10^{10} \text{ m}^3 \text{ s}^{-2}$ (GFDL_D) and for cluster 4 it varies between 1.5×10^{10} (CMCC_D) and $2.9 \times 10^{10} \text{ m}^3 \text{ s}^{-2}$ (GFDL_D), in observations the mean PDI values are 4.0 and $2.8 \times 10^{10} \text{ m}^3 \text{ s}^{-2}$, respectively. The mean PDI per tropical cyclone depends on the tropical cyclone duration and intensity. Because all the downscaled models overestimate the storm duration and underestimate the storm intensity, the bias in mean PDI per storm can be attributed to the bias in storm intensity (Table 5). In observations, cluster 3 tropical cyclones have the highest value of mean PDI (Table 5) and hence are potentially more dangerous when reaching the coasts. Except for CAM5_D, the downscaled models reproduce the higher mean PDI of cluster 3 tropical cyclones (Table 5). This is an important result, because it is fundamental to be able to simulate well the characteristics of the most potentially destructive storms.

Similarly, for the observed total PDI (Table 5), cluster 3 has a much higher value than the others, reaching

$850 \times 10^{10} \text{ m}^3 \text{ s}^{-2}$ with the second highest value ($314 \times 10^{10} \text{ m}^3 \text{ s}^{-2}$) occurring in cluster 4. Unfortunately, except CMCC_D, none of the downscaled models reproduces this characteristic, because of an underestimation of the intensity and wrong proportion of tropical cyclones per cluster (Table 5). For GFDL_D, cluster 1 presents the highest total PDI, overestimating of intensity and proportion (Table 5) of the total PDI in that cluster. For CAM5_D and GISS_D, clusters 4 and 2 are respectively the ones with the highest total PDI among all clusters, overestimating the proportion of tropical cyclones in those clusters.

c. Landfalls

Besides specific intensity, frequency and duration characteristics, Kossin et al. (2010) showed that observed clusters present different landfall properties. To obtain the points of landfall for each model, we first used a very high-resolution land–sea mask based on observational data in order to include all small islands. Then we interpolated each track from 6-hourly positions to 15-min increments using cubic splines. Finally, for each interpolated track, whenever the storm location is over land—and on the previous time step the storm was over water—this is defined as a landfall. Characteristics of landfalls are very important in climate studies, as land-falling storms can impact the coastal population. Therefore, the ability of climate models to reproduce landfall distribution and robust projections of changes in landfall frequency is essential for impact studies.

Table 5 presents the number and proportion of landfalls in observations and downscaled simulations for each cluster. The downscaled simulations have very realistic landfall proportions compared to observations, with most of the tropical cyclones in clusters 2 and 4 making landfall at least once, while the landfall proportion in clusters 1 and 3 is much lower because of the eastern genesis location of the last two clusters.

The clusters differ not only in landfall proportions but also more importantly on the geographic position of their landfalls (as shown in observations in right panels of Fig. 1). Observed and downscaled tropical cyclones in cluster 1 make landfall along the eastern U.S. and Canada coasts. Cluster 2 landfalls are largely confined to the Gulf of Mexico, western Caribbean, and Antilles, whereas cluster 3 landfalls occur over the eastern U.S. and Canada coasts and the Antilles. Finally, cluster 4 has the landfalls in the Antilles and the Mexico and Central America coasts. There is a much higher proportion of tracks making landfall in the eastern U.S. and Canada coasts in the downscaled models compared to the observations for all the clusters.

Another important characteristic to consider is the ability of models to simulate the intensity of storms at

landfall, which is shown in Table 5 for observations and downscaled models for each cluster. The southernmost tropical cyclones have higher intensity at landfall for the observations and in two of the downscaled models (CAM5_D and GISS_D). In contrast, CMCC_D and GFDL_D present very similar intensities at landfall for all clusters. The reasons for these differences should be addressed in a future study.

d. Seasonality

The seasonality of downscaled simulations for all storms in the basin is very similar to observations (not shown). However, as shown in Fig. 9, none of the downscaled models is able to reproduce the observed seasonal distribution per cluster. Also, as in Fig. 7, the large error bars show that the models have very large spread among them. For GFDL_D (Fig. 9c) and GISS_D (Fig. 9d), one cluster is prevalent: cluster 1 is highly dominant for GFDL_D in the early and the middle part of the season, while for GISS_D cluster 2 has larger values over the whole season. In those two cases, the dominant cluster has also a largely overestimated proportion (Table 5). For CAM5_D (Fig. 9a) and CMCC_D (Fig. 9b), there is a different leading cluster in each part of the season, but these are different from observations.

It is interesting to note that, except CAM5_D, the seasonal cycle of explicit versus downscaled simulations is completely different (cf. Figs. 7b and 9a). Moreover, while GFDL_E had a realistic seasonal cycle per cluster (Fig. 7d), when using the downscaling technique, the seasonal cycle of GFDL_D is degraded (Fig. 9c). The biases of this downscaled model cannot be attributed to the large-scale conditions as these two simulations share the same large-scale environment. The seeding process, as well as the seeding timing, could be a possible explanation for the differences between the seasonality in explicit and downscaled simulations. As mentioned above, one drawback of the downscaling method is that there is no link with the timing of the African easterly waves; this could be one of reasons for seasonality biases of the downscaled simulations, especially in the case of the nonrealistic timing of genesis of cluster 3 storm genesis. This result clearly shows a limitation of the downscaling technique that should be further improved.

In summary, the downscaled models generally simulate better the cluster separation and characteristics, such as duration, intensity, PDI, and landfalls frequency, when compared with explicit models; in particular, the storms reach the intensity of hurricanes and major hurricanes. However, there are some biases remaining. For example, some of the downscaled models are not able to reproduce the bimodal distribution of intensity between the northernmost and southernmost tropical cyclones

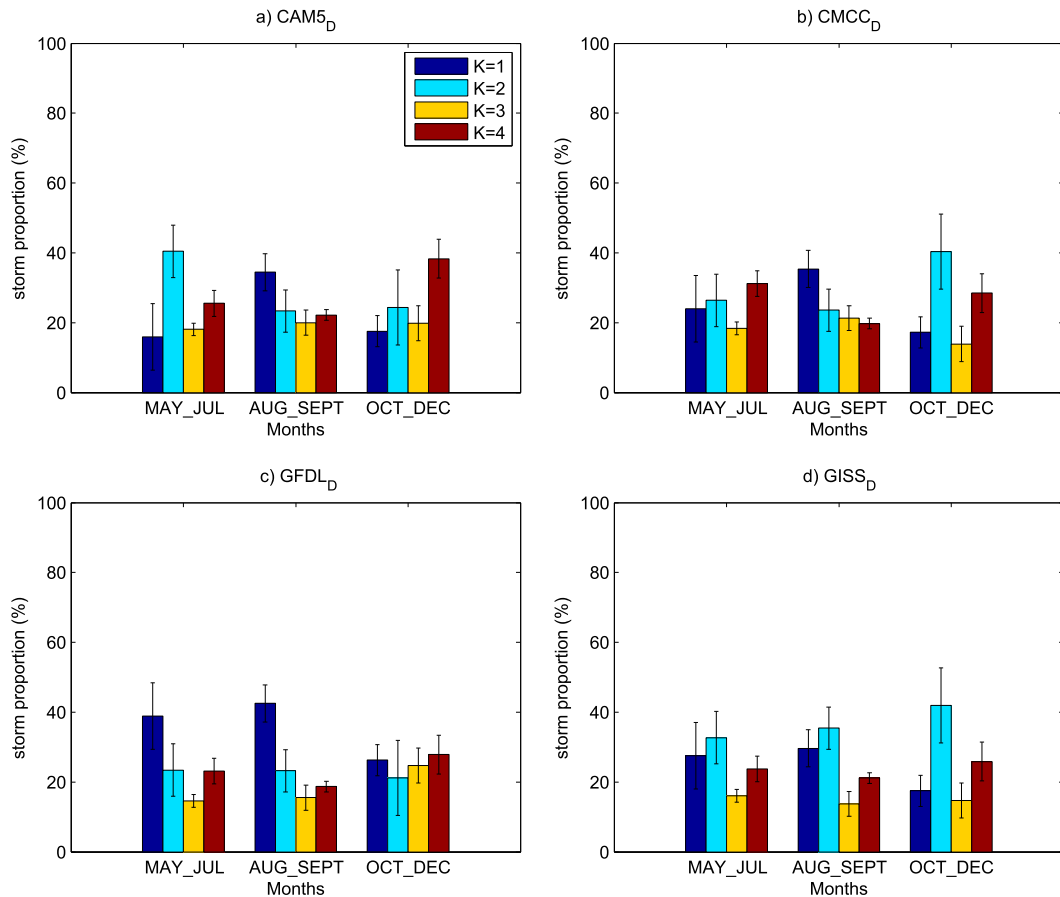


FIG. 9. As in Fig. 7, but for the downscaled simulations.

and all downscaled models had problems simulating the seasonality of cluster memberships.

5. Future changes in North Atlantic tracks

a. Frequency

Because of the low number of tropical cyclones in most of the explicit models, future changes in tropical cyclone activity are only examined for the downscaled models. The histograms in Fig. 10 show the difference in the number of tropical cyclones per year for each of the three perturbation experiments (p2K = 2-K increase in SST, 2CO₂ = 2 × CO₂, and p2K2CO₂ = 2-K increase in SST and 2 × CO₂). The results are shown for the cluster memberships, as well as the total number of tropical cyclones. Error bars indicate the 90% confidence interval on the differences. A Student's *t* test was realized in order to get the confidence intervals.

The changes in the total number of tropical cyclones per year show large differences among the four downscaled models, as well as the three idealized scenarios. CAM5_D and CMCC_D both show an increase of the

total number of tropical cyclone per year, for all the scenarios. One reason for that might be that, if the same seeding rate is kept between the present and future simulations, under future conditions the environment might more favorable so the number of tropical cyclones might get higher. However, for CAM5_D, the results are not statistically significant. In the case of CMCC_D, there is a major significant increase in tropical cyclone frequency for all scenarios: +45% (p2K; Fig. 10a), +27% (2CO₂; Fig. 10b), and +22% (p2K2CO₂; Fig. 10c), respectively. In contrast, the other downscaled models tend to present weaker changes and often differ in sign. For the p2K scenario (Fig. 10a), GFDL_D and GISS_D show significant decreases in frequency of tropical cyclones per year with −9% and −6%, respectively. For the 2CO₂ (Fig. 10b) and p2K2CO₂ (Fig. 10c) scenarios, GFDL_D and GISS_D also present decreases in tropical cyclone frequency; however, changes in GFDL_D are not statistically significant. GISS_D has small decreases of number of tropical cyclones per year with −3% for 2CO₂ and −6% for p2K2CO₂. Yoshimura and Sugi (2005) showed that frequency changes in the

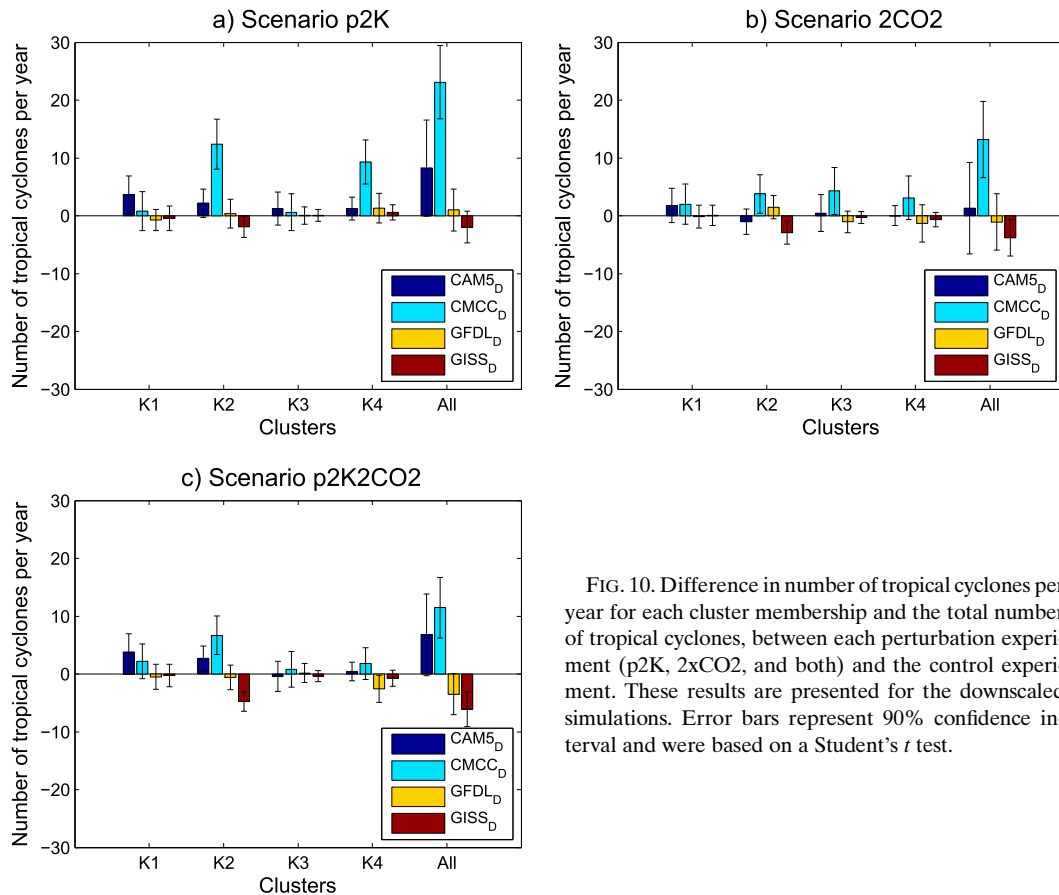


FIG. 10. Difference in number of tropical cyclones per year for each cluster membership and the total number of tropical cyclones, between each perturbation experiment (p2K, 2xCO₂, and both) and the control experiment. These results are presented for the downscaled simulations. Error bars represent 90% confidence interval and were based on a Student's *t* test.

p2K2CO₂ scenario are mainly coming from the increase in CO₂ concentration. On the other hand, Held and Zhao (2011) showed similar levels of contribution from SST and CO₂ in the reduction of tropical cyclone frequency. However, these two studies were performed at a global scale, so they do not necessarily apply to the North Atlantic basin. In our case, it is not really easy to identify the proportions in the contribution of SST or CO₂ to the p2K2CO₂ scenario. More details on the different roles of SST warming and the CO₂ increase in future changes in tropical cyclone activity are currently being investigated by Zhao et al. (2013), as part of the effort of the U.S. CLIVAR Hurricane Working Group.

Regarding future changes of the cluster memberships, for all the downscaled simulations and nearly all the scenarios, the main changes in tropical cyclone frequency come from the northernmost tropical cyclones (clusters 1 and 2). More concretely, for GFDL_D and GISS_D this means a decrease of the number of tropical cyclones over the western part of the North Atlantic basin, a pattern that has already been observed in several previous studies (Chauvin et al. 2006; Murakami

and Wang 2010; Caron et al. 2011; Zhao and Held 2012). These studies also project an increase of activity over the eastern Atlantic, which is not present in GFDL_D and GISS_D. On the other hand, CAM5_D and CMCC_D have an increase in the northernmost tropical cyclones. In the case of CMCC_D, the increase is also occurring for the southernmost tropical cyclones: that is, an increase of tropical cyclones over the entire North Atlantic basin, which agrees with other studies, such as Oouchi et al. (2006) and Emanuel (2013), and a few of the models examined in Camargo (2013).

b. Intensity

Figure 11 shows the fraction changes in LMI. Similar to future frequency changes (section 5a), the changes in intensity (LMI) depend on the model and the scenario examined. The downscaled models show a robust increase of the intensity of tropical cyclones in the p2K scenario for all models, but with different rates (Fig. 11a). GFDL_D and GISS_D have a weak increase (under 3 m s⁻¹), while for CAM5_D and CMCC_D the increase is stronger, reaching approximately 3 and 5 m s⁻¹, respectively, and is statistically significant. In contrast for

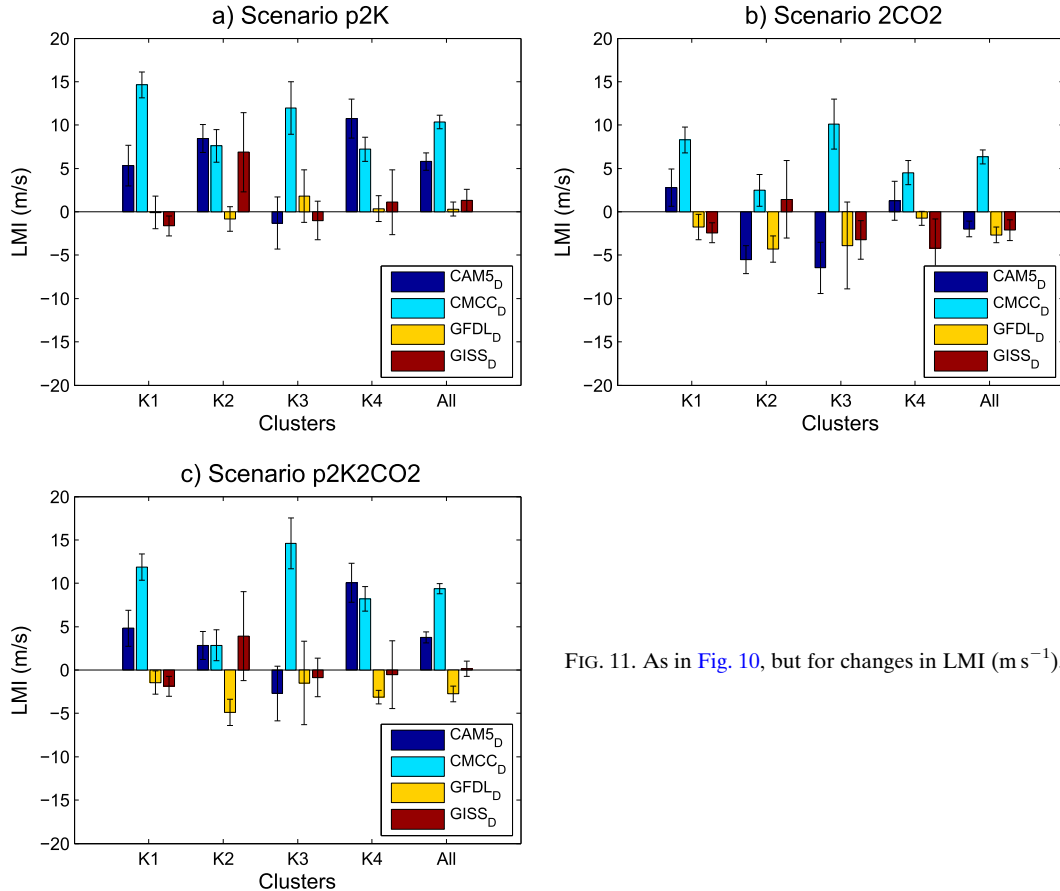


FIG. 11. As in Fig. 10, but for changes in LMI (m s^{-1}).

the 2CO2 (Fig. 11b) and p2K2CO2 (Fig. 11c) scenarios, the models show significant but incoherent results. While three of the models (CAM5_D, GFDL_D, and GISS_D) show a moderate decrease in intensity ($< -5 \text{ m s}^{-1}$), CMCC_D has an increase of 7 m s^{-1} for the 2CO2 scenario. In the p2K2CO2 scenario, GFDL_D has a moderate decrease, GISS_D has no changes, and CAM5_D and CMCC_D have an increase in intensity: ~ 5 and 10 m s^{-1} , respectively. Held and Zhao (2011) found that the increase in the average intensity of tropical cyclones is mostly due to the SST warming. In our case, not all the simulations show an increase in intensity and it is not possible to identify which factor is the most important between SST and CO₂. Indeed, the results are hardly significant for three of the models when the effects of SST and CO₂ are examined individually. In the case of CMCC_D, the results are significant but very similar between the two scenarios, which again does not let us identify which parameter is the most important for the intensity changes. An important point is that, in contrast to the tropical cyclone frequency changes, it is not possible to identify which clusters are responsible for the changes in intensity

changes: that is, all the simulations the changes are distributed among at least three clusters.

6. Summary and discussion

In this paper, we analyzed the simulations of the U.S. CLIVAR Hurricane Working Group in order to study the ability of explicit and downscaled models to represent the tropical cyclone cluster tracks over the North Atlantic basin. As mentioned earlier, this analysis is a tentative study as we were facing some limitations because of the differences in tracking algorithms. Thus, the results should be considered preliminary. The results show, first, the examination of the climatologies of the tropical cyclone clusters in nine different climate models. With the exception of GFDL_E, the explicit simulations are not able to reproduce all the cluster types, but most of them simulate realistically at least three of the four clusters. Many models have problems simulating clusters 3 and 4 storms: that is, the southernmost tropical cyclones. This bias can be directly related to the realism of the African easterly wave activity for one model and an unfavorable environment created by high values of

vertical wind shear for a few specific models. This can also be due to the fact that models often have an insufficient representation of the storms in the tropics so the peak in intensity is not reached until they reach higher latitudes.

The climatological clusters of the storms explicitly generated by climate models show strong biases in storm intensity and mean PDI per storm. The different characteristics in these variables between the northernmost (clusters 1 and 2) and southernmost observed tropical cyclones (clusters 3 and 4) (Kossin et al. 2010) are not present in the explicit simulations. Furthermore, the intensity of the tropical cyclones is still underestimated in many models confirming the need for high-resolution models for studying tropical cyclone activity, though this is not sufficient, as some high-resolution models still cannot simulate the most intense storms.

In the second part of this paper, the downscaling technique of Emanuel et al. (2008) was applied to the output of four climate models from the previous section. The results show that, apart from the seasonality, the downscaled models are better able to reproduce the observed characteristics compared to the explicit model results. However, the explicit models have limitations, especially in the way the tropical cyclones are detected. The downscaled models have a realistic representation of the tracks, genesis, and landfalls patterns. They also manage to reproduce many of the characteristics of cluster memberships, such as a distinction between the northernmost and southernmost tropical cyclones in terms of mean duration, intensity, and PDI. In addition, most of the downscaled models present a realistic proportion of landfalls as well as major (categories 3–5) and category 5 hurricanes. Improvements can still be made on the downscaled models regarding seasonality, as the seasonal cycle of individual clusters is not accurately simulated. For example, modifying the seeding technique taking in account the seasonality of African easterly wave activity could lead to significant improvements.

It should be noted that the models examined here are forced with climatological SST, so they do not have any information on interannual variability, in contrast to the observations. This fact could potentially explain some of the differences between the simulations and the observations encountered in this paper. Kossin et al. (2010) demonstrated that factors such as ENSO, the AMM, or the North Atlantic Oscillation (NAO) highly modulate the cluster membership.

The last part of the paper aims to study the impacts of warming of SST and increase in CO₂ rate on the characteristics of the tropical cyclones clusters. The results are not robust among the four downscaled simulations. Two of the four downscaled simulations show a decrease in tropical cyclone frequency in the p2K2CO₂ scenario,

with only one presenting significant increase, while the two others show a small increase. Contrarily to previous studies (Yoshimura and Sugi 2005; Held and Zhao 2011), it is not possible to identify the proportion of the contributions of the p2K and 2CO₂ scenarios to future changes. However, models are in agreement that the frequency changes are due to the northernmost tropical cyclones. Concerning the intensity, all the models agree on an increase for the scenario with a warming of SST, with most models showing a significant increase of intensity. For the two other scenarios, the four simulations do not agree, showing different signs of intensity changes, and it is not possible to identify specific clusters responsible for these changes. The only differences among the downscaled models are in the large-scale environmental fields, which lead to very different projections in tropical cyclone frequency changes. These large differences in projections are representative of how difficult it is to assess future changes of tropical cyclone activity, especially in regional scales, and show that we need to be very careful when reaching conclusions analyzing a single climate model, pointing to the advantages of multimodel intercomparison projects, as well as the need for ensemble simulations.

In the future, it would be important to repeat this analysis using a more comparable dataset, in which a common tracking algorithm is used. Alternatively, the sensitivity to various tracking algorithms could be tested on a common data such as a reanalysis dataset.

Acknowledgments. We acknowledge support from NOAA Grant NA11OAR4310093, NSF Grant AGS1143959, and NASA Grant NNX09AK34G. The data were provided by the U.S. CLIVAR Hurricane Working Group. We thank Naomi Henderson for her support with the U.S. CLIVAR Hurricane Working Group dataset. Wehner was supported by the Regional and Global Climate Modeling Program of the Office of Biological and Environmental Research in the Department of Energy Office of Science under Contract DE-AC02-05CH11231. CAM5 calculations were performed at the National Energy Research Supercomputing Center (NERSC) at the Lawrence Berkeley National Laboratory. We also would like to thank the three anonymous reviewers for their helpful comments.

APPENDIX

Description of the Detection of Tropical Cyclones in Simulations

For the downscaled simulations, the seeds are not considered to form tropical cyclones unless they develop winds of at least 21 m s⁻¹.

For the explicit simulations, the tracking algorithms employed in this study are described for each model here. Table A1 also presents the variables and the thresholds chosen for each technique.

For CAM5_E, the tracking algorithm used is described in Knutson et al. (2007). The following criteria were employed:

- (i) A local relative vorticity maximum at 850 hPa exceeds $1.6 \times 10^{-4} \text{ s}^{-1}$.
- (ii) The surface pressure increases by at least 4 hPa from the storm center within a radius of 5° . The closest local minimum in sea level pressure within a distance of 2° latitude or longitude from the vorticity maximum is defined as the center of the storm.
- (iii) The distance of the warm-core center from the storm center does not exceed 2° . The temperature decreases by at least 0.8°C in all directions from the warm-core center within a distance of 5° . The closest local maximum in temperature averaged between 300 and 500 hPa is defined as the center of the warm core.

Maxima and minima are located, and gradients are evaluated using bicubic splines, which provide higher precision than the model resolution.

For WRF_E, the tracking algorithm follows the one from Walsh (1997). The criteria we used include the following:

- (i) a minimum 850-hPa relative vorticity of $2 \times 10^{-4} \text{ s}^{-1}$;
- (ii) A closed minimum in sea level pressure within 2.5° of the point identified in (i);
- (iii) 10-m wind speed of at least 17.5 m s^{-1} ;
- (iv) warm-core criteria described in Walsh (1997);
- (v) mean wind speed around the center of the storm (2.5° on each side) at 850 hPa must be higher than at 300 hPa;
- (vi) tropical cyclone exists for at least 2 days; and
- (vii) tropical cyclone origin is south of 30°N .

GFDL_E and GFS_E follow the same algorithm as Zhao et al. (2009), which identifies tropical cyclones by locating grid points meeting the following criteria:

- (i) $3.5 \times 10^{-5} \text{ s}^{-1}$ within a $6^\circ \times 6^\circ$ latitude/longitude box;
- (ii) a local minimum of sea level pressure within 2° latitude/longitude from the vorticity maximum; and
- (iii) a local maximum anomaly in the temperature averaged between 300 and 500 hPa located within 2° of SLP minimum, where the TEMPERATURE must be at least 1°C warmer than the surrounding local mean.

For the simulations from HG3A_E, the tracking algorithm follows previous studies (Hodges 1999, Bengtsson et al. 2007), as explained in Strachan et al. (2013):

TABLE A1. Description of the fields and levels used in the tracking algorithms.

Model/tracking Scheme	Variables and levels selected
CAM5_E/Knutson et al. (2007)	Relative vorticity: 850 hPa Surface pressure Temperature: 300 and 500 hPa
WRF_E/Walsh (1997)	Relative vorticity: 850 hPa Surface pressure Wind speed: 10 m, 850 hPa, and 300 hPa
GFDL_E /GFS_E/Zhao et al. (2009)	Temperature: 700, 500, and 300 hPa Relative vorticity: 850 hPa Surface pressure Temperature: 300 and 500 hPa
HG3A_E/Strachan et al. (2013)	T42 relative vorticity: 850 hPa T63 vorticity: 850, 500, 300, and 200 hPa
CMCC_E/Zhao et al. (2009)	Relative vorticity: 850 hPa Surface pressure Wind velocity: 300 and 850 hPa Temperature: 700, 500, and 300 hPa
GSFC_E/Vitart et al. (2003)	Relative vorticity: 850 hPa Surface pressure Temperature levels: 500 and 200 hPa
GISS_E/Camargo and Zebiak (2002)	Relative vorticity: 850 hPa Surface pressure Temperature: 850, 700, 500, and 300 hPa Wind speed: 850 and 300 hPa
FSU_E/LaRow et al. (2008)	Relative vorticity: 850 hPa Surface pressure Temperature: 500 and 200 hPa
Horn et al. (2013)	Absolute vorticity: 850 hPa Surface pressure Wind speed: 10 m, 850 hPa, and 300 hPa Temperature: 300 hPa

- (i) Maxima in 850 hPa spectrally filtered to T42 vorticity greater than $0.5 \times 10^{-5} \text{ s}^{-1}$ are tracked.
- (ii) Lifetime is greater than 2 days.
- (iii) T63 relative vorticity at 850 hPa must be superior or equal to $6 \times 10^{-5} \text{ s}^{-1}$ during track obtained above.
- (iv) Positive T63 vorticity center must exist at 850, 500, 300, and 200 hPa.
- (v) There must be a reduction of at least $6 \times 10^{-5} \text{ s}^{-1}$ in vorticity between 850 and 200 hPa as evidence of a warm core.
- (vi) There must be a reduction in T63 vorticity with height checked between each pair of 850-, 500-, 300-, and 200-hPa levels.
- (vii) Conditions iii–vi must be attained for at least 1 day.

For CMCC_E, their tracking scheme has been developed based on the one developed by Walsh (1997). Six criteria are defined as follows:

- (i) Relative vorticity at 850 hPa is larger than $1.0 \times 10^{-5} \text{ s}^{-1}$.
- (ii) There is a relative surface pressure minimum, and the surface pressure anomaly, compared to a surrounding area with a radius of 350 km, is larger than 2 hPa.
- (iii) In a region with a radius of 350 km around the grid point considered, there is a grid point where the maximum surface wind velocity is larger than 15.5 m s^{-1} .
- (iv) Wind velocity at 850 hPa is larger than wind velocity at 300 hPa.
- (v) The sum of temperature anomalies at 700, 500, and 300 hPa is larger than 1 K, where anomalies are defined as the deviation from a spatial mean computed over a region with a radius of 350 km.
- (vi) The above-mentioned conditions persist for at least 24 h (corresponding to four time steps of the model output).

For GSFC_E, the tracking scheme is similar to one from Vitart et al. (2003). The criteria are defined as follows:

- (i) Local relative vorticity maximum is greater than $3.5 \times 10^{-5} \text{ s}^{-1}$ at 850-hPa level.
- (ii) Warm core: From the center of the tropical cyclone, the temperature must decrease by at least 6 K in all directions within a distance of 4° .
- (iii) The distance between the tropical cyclone center and the center of the warm core must not exceed 2° longitude and latitude.
- (iv) The minimum sea level pressure defines the center of the tropical cyclone and must exist within $2^\circ \times 2^\circ$ radius of the vorticity maximum.

For GISS_E, the tracking scheme of Camargo and Zebiak (2002) has been used. Based on the analysis of the joint probability distribution functions obtained in the 850-hPa relative vorticity, the 850–300-hPa anomalous integrated temperature, and the surface wind speed for climate models, the following model-dependent criteria are chosen:

- (i) 850-hPa relative vorticity at least twice the standard deviation of the vorticity;
- (ii) 830–300-hPa anomalous integrated temperature threshold greater than or equal to the standard deviation calculated over only those cases where there is a warm core; and
- (iii) surface wind speed greater than or equal to the global average wind speed (over ocean only) plus the standard deviation in the relevant basin.

The scheme also imposes the following mode-independent criteria:

- (i) a local minimum in mean sea level pressure;
- (ii) a positive local temperature only at 850, 700, 500, and 300 hPa;
- (iii) a larger local temperature anomaly at 850 hPa than at 300 hPa; and
- (iv) higher mean wind speeds at 850 hPa than at 300 hPa.

Successive detections are connected into tracks if they are within 5° of each other. Tracks of at least 1.5 days are considered to be tropical cyclones. These tracks are then extended forward and backward in time by tracking the vorticity maximum while the absolute value exceeds a relaxed vorticity threshold. This is intended to achieve more realistic track lengths.

The scheme for FSU_E is described in LaRow et al. (2008) and identifies tropical cyclones by locating grid points meeting the following criteria:

- (i) $1.0 \times 10^{-4} \text{ s}^{-1}$ at 850 hPa within a $4^\circ \times 4^\circ$ latitude/longitude box;
- (ii) a local minimum of sea level pressure within 2° latitude/longitude from the vorticity maximum; and
- (iii) a local maximum anomaly in the temperature averaged between 200 and 500 hPa located within 2° of sea level pressure minimum, where temperature must be at least 3°C warmer than the surrounding local mean.

For testing the sensitivity of the cluster analysis to the tracking techniques, we also used the tracking algorithm of the modified Commonwealth Scientific and Industrial Research Organization (CSIRO) tracking scheme (Walsh et al. 2007; Horn et al. 2013). The scheme uses the following criteria to locate tropical cyclones:

- (i) an absolute value of 850-hPa vorticity greater than 10^{-5} s^{-1} ;
- (ii) a closed pressure minimum within a distance in both the x and y directions of 350 km from a point satisfying condition 1 (distance chosen empirically to give a good geographical association between vorticity maxima and pressure minima), where this minimum pressure is taken as the center of the storm;
- (iii) a mean wind speed in the region $700 \text{ km} \times 700 \text{ km}$ around the center of the storm at 850 hPa greater than at 300 hPa;
- (iv) a temperature anomaly at the center of the storm at 300 hPa greater than zero; and
- (v) maximum 10-m wind speeds exceeding a resolution-dependent value as specified in Walsh et al. (2007).

Detections are allowed only over ocean, based on topography fields degraded to model resolution, unless

previous detection exists within a resolution-dependent distance. These detections are then linked into tracks by associating consecutive detections within 6° of each other. Tracks lasting less than 24 h are excluded. No latitude restriction is imposed and the tropical cyclones are instead partitioned from extratropical storms using the separation in the latitudinal distribution of their genesis points caused by the extratropical ridges in both hemispheres. This is one point of departure from the original CSIRO scheme; another is the removal of a computationally demanding warm-core check that was found to be unnecessary at the higher resolutions used in the CLIVAR experiments (Horn et al. 2013).

REFERENCES

- Anderson, J. L., and Coauthors, 2004: The new GFDL global atmosphere and land model AM2/LM2: Evaluation with prescribed SST simulations. *J. Climate*, **17**, 4641–4673, doi:10.1175/JCLI-3223.1.
- Bain, C. L., K. D. Williams, S. F. Milton, and J. T. Heming, 2014: Objective tracking of African easterly waves at the Met Office models. *Quart. J. Roy. Meteor. Soc.*, **140**, 47–57, doi:10.1002/qj.2110.
- Bengtsson, L., K. I. Hodges, M. Esch, N. Keenlyside, L. Kornbluh, J. Luo, and T. Yamagata, 2007: How may tropical cyclones change in a warmer climate? *Tellus*, **59A**, 539–561, doi:10.1111/j.1600-0870.2007.00251.x.
- Bracken, W. E., and L. F. Bosart, 2000: The role of synoptic-scale flow during tropical cyclogenesis over the North Atlantic Ocean. *Mon. Wea. Rev.*, **128**, 353–376, doi:10.1175/1520-0493(2000)128<0353:TROSSF>2.0.CO;2.
- Camargo, S. J., 2013: Global and regional aspects of tropical cyclone activity in the CMIP5 models. *J. Climate*, **26**, 9880–9902, doi:10.1175/JCLI-D-12-00549.1.
- , and S. E. Zebiak, 2002: Improving the detection and tracking of tropical cyclones in atmospheric general circulation models. *Wea. Forecasting*, **17**, 1152–1162, doi:10.1175/1520-0434(2002)017<1152:ITDATO>2.0.CO;2.
- , A. G. Barnston, and S. E. Zebiak, 2005: A statistical assessment of tropical cyclone activity in atmospheric general circulation models. *Tellus*, **57A**, 589–604, doi:10.1111/j.1600-0870.2005.00117.x.
- , A. W. Robertson, S. J. Gaffney, P. Smyth, and M. Ghil, 2007: Cluster analysis of typhoon tracks. Part II: Large-scale circulation and ENSO. *J. Climate*, **20**, 3654–3676, doi:10.1175/JCLI4203.1.
- , —, A. G. Barnston, and M. Ghil, 2008: Clustering of eastern North Pacific tropical cyclone tracks: ENSO and MJO effects. *Geochim. Geophys. Geosyst.*, **9**, Q06V05, doi:10.1029/2007GC001861.
- Caron, L. P., C. Jones, and K. Winger, 2011: Impact of resolution and downscaling technique in simulating recent tropical cyclone activity. *Climate Dyn.*, **37**, 869–892, doi:10.1007/s00382-010-0846-7.
- Chand, S. S., and K. J. E. Walsh, 2009: Tropical cyclone activity in the Fiji region: Spatial patterns and relationship to large-scale circulation. *J. Climate*, **22**, 3877–3893, doi:10.1175/2009JCLI2880.1.
- Chauvin, F., J. F. Royer, and M. Déqué, 2006: Response of hurricane-type vortices to global warming as simulated by ARPEGE-Climat at high resolution. *Climate Dyn.*, **27**, 377–399, doi:10.1007/s00382-006-0135-7.
- Cocke, S., and T. E. LaRow, 2000: Seasonal predictions using a regional spectral model embedded within a coupled ocean–atmosphere model. *Mon. Wea. Rev.*, **128**, 689–708, doi:10.1175/1520-0493(2000)128<0689:SPUARS>2.0.CO;2.
- Colbert, J. A., B. J. Soden, G. A. Vecchi, and B. P. Kirtman, 2013: The impact of anthropogenic climate change on North Atlantic tropical cyclone tracks. *J. Climate*, **26**, 4088–4095, doi:10.1175/JCLI-D-12-00342.1.
- Daloz, A. S., F. Chauvin, K. Walsh, S. Lavender, D. Abbs, and F. Roux, 2012: The ability of general circulation models to simulate tropical cyclones and their precursors over the North Atlantic main development region. *Climate Dyn.*, **39**, 1559–1576, doi:10.1007/s00382-012-1290-7.
- Dee, D. P., and Coauthors, 2011: The ERA-Interim reanalysis: Configuration and performance of the data assimilation system. *Quart. J. Roy. Meteor. Soc.*, **137**, 553–597, doi:10.1002/qj.828.
- Elsner, J. B., J. P. Kossin, and T. H. Jagger, 2008: The increasing intensity of the strongest tropical cyclones. *Nature*, **455**, 92–95, doi:10.1038/nature07234.
- Emanuel, K., 2005: Increasing destructiveness of tropical cyclones over the past 30 years. *Nature*, **436**, 686–688, doi:10.1038/nature03906.
- , 2006: Climate and tropical cyclone activity: A new model downscaling approach. *J. Climate*, **19**, 4797–4802, doi:10.1175/JCLI3908.1.
- , 2010: Tropical cyclone activity downscaled from NOAA-CIRES reanalysis, 1908–1958. *J. Adv. Model. Earth Syst.*, **2**, doi:10.3894/JAMES.2010.2.1.
- , 2013: Downscaling CMIP5 climate models show increased tropical cyclone activity over the 21st century. *Proc. Natl. Acad. Sci. USA*, **110**, 12 219–12 224, doi:10.1073/pnas.1301293110.
- , C. DesAutels, C. Holloway, and R. Korty, 2004: Environmental control of tropical cyclone intensity. *J. Atmos. Sci.*, **61**, 843–858, doi:10.1175/1520-0469(2004)061<0843:ECOTCI>2.0.CO;2.
- , S. Ravela, E. Vivant, and C. Risi, 2006: A statistical deterministic approach to hurricane risk assessment. *Bull. Amer. Meteor. Soc.*, **87**, 299–314, doi:10.1175/BAMS-87-3-299.
- , R. Sundararajan, and J. Williams, 2008: Hurricanes and global warming: Results from downscaling IPCC AR4 simulations. *Bull. Amer. Meteor. Soc.*, **89**, 347–367, doi:10.1175/BAMS-89-3-347.
- , K. Oouchi, M. Satoh, H. Tomita, and Y. Yamada, 2010: Comparison of explicitly simulated and downscaled tropical cyclone activity in a high-resolution global climate model. *J. Adv. Model Earth Syst.*, **2**, doi:10.3894/JAMES.2010.2.9.
- Fyfe, J. C., 1999: Climate simulations of African easterly waves. *J. Climate*, **12**, 1747–1769, doi:10.1175/1520-0442(1999)012<1747:CSOAEW>2.0.CO;2.
- Gaffney, S. J., A. W. Robertson, P. Smyth, S. J. Camargo, and M. Ghil, 2007: Probabilistic clustering of extratropical cyclones using regression mixture models. *Climate Dyn.*, **29**, 423–440, doi:10.1007/s00382-007-0235-z.
- Gray, W. M., 1968: A global view of the origin of tropical disturbances and storms. *Mon. Wea. Rev.*, **96**, 669–700, doi:10.1175/1520-0493(1968)096<0669:GVOTOO>2.0.CO;2.
- Gualdi, S., E. Scoccimarro, and A. Navarra, 2008: Changes in tropical cyclone activity due to global warming: Results from a high-resolution coupled general circulation model. *J. Climate*, **21**, 5204–5228, doi:10.1175/2008JCLI1921.1.
- Held, I. M., and M. Zhao, 2011: The response of tropical cyclone statistics to an increase in CO₂ with fixed sea surface

- temperatures. *J. Climate*, **24**, 5353–5364, doi:10.1175/JCLI-D-11-00050.1.
- Hodanish, S. J., and W. Gray, 1993: An observational analysis of tropical cyclone recurvature. *Mon. Wea. Rev.*, **121**, 2665–2689, doi:10.1175/1520-0493(1993)121<2665:AOATC>2.0.CO;2.
- Hodges, K. I., 1999: Adaptive constrains for feature tracking. *Mon. Wea. Rev.*, **127**, 1362–1373, doi:10.1175/1520-0493(1999)127<1362:ACFFT>2.0.CO;2.
- Horn, M., K. Walsh, and A. Ballinger, 2013: Detection of tropical cyclones using a phenomenon-based cyclone tracking scheme. *Proc. U.S. CLIVAR Hurricane Workshop*, Princeton, NJ, Geophysical Fluid Dynamics Laboratory, 27 pp. [Available online at http://www.usclivar.org/sites/default/files/meetings/Walsh_clivar_gfdl_2013.pdf.]
- , and Coauthors, 2014: Tracking scheme dependence of simulated tropical cyclone response to idealized climate simulations. *J. Climate*, **27**, 9197–9213, doi:10.1175/JCLI-D-14-00200.1.
- Jarvinen, B. R., C. J. Neumann, and M. A. S. Davis, 1984: A tropical cyclone data tape for the North Atlantic basin, 1886–1983: Contents, limitations, and uses. NOAA Tech. Memo. NWS NHC-22, 21 pp.
- Kalnay, E., and Coauthors, 1996: The NCEP/NCAR 40-Year Reanalysis Project. *Bull. Amer. Meteor. Soc.*, **77**, 437–471, doi:10.1175/1520-0477(1996)077<0437:TNYRP>2.0.CO;2.
- Kim, D., A. H. Sobel, A. D. Del Genio, Y. Chen, S. J. Camargo, M.-S. Yao, M. Kelley, and L. Nazarenko, 2012: The tropical subseasonal variability simulated in the NASA GISS general circulation model. *J. Climate*, **25**, 4641–4659, doi:10.1175/JCLI-D-11-00447.1.
- Knutson, T. R., J. J. Sirutis, S. T. Garner, I. M. Held, and R. E. Tuleya, 2007: Simulation of the recent multidecadal increase of Atlantic hurricane activity using an 18-km-grid regional model. *Bull. Amer. Meteor. Soc.*, **88**, 1549–1565, doi:10.1175/BAMS-88-10-1549.
- , and Coauthors, 2010: Tropical cyclones and climate change. *Nat. Geosci.*, **2**, 157–163, doi:10.1038/ngeo779.
- Kossin, J. P., S. J. Camargo, and M. Sitkowski, 2010: Climate modulation of North Atlantic hurricane tracks. *J. Climate*, **23**, 3057–3076, doi:10.1175/2010JCLI3497.1.
- Landsea, C. W., 1993: A climatology of intense (or major) Atlantic hurricanes. *Mon. Wea. Rev.*, **121**, 1703–1713, doi:10.1175/1520-0493(1993)121<1703:ACOIMA>2.0.CO;2.
- , G. A. Vecchi, L. Bengtsson, and T. R. Knutson, 2010: Impact of the duration thresholds on Atlantic tropical cyclone counts. *J. Climate*, **23**, 2508–2519, doi:10.1175/2009JCLI3034.1.
- LaRow, T. E., Y. K. Lim, D. W. Shin, E. Chassignet, and S. Cocke, 2008: Atlantic basin seasonal hurricane simulations. *J. Climate*, **21**, 3191–3206, doi:10.1175/2007JCLI2036.1.
- Lin, N., K. Emanuel, M. Oppenheimer, and E. Vanmarcke, 2012: Physically based assessment of hurricane surge threat under climate change. *Nat. Climate Change*, **2**, 462–467, doi:10.1038/nclimate1389.
- Manganello, J., and Coauthors, 2012: Tropical cyclone climatology in a 10-km global atmospheric GCM: Toward weather-resolving climate modeling. *J. Climate*, **25**, 3867–3893, doi:10.1175/JCLI-D-11-00346.1.
- McTaggart-Cowan, R., G. D. Deane, L. F. Bosart, C. A. Davies, and T. J. Galarneau, 2008: Climatology of the tropical cyclogenesis in the North Atlantic (1948–2004). *Mon. Wea. Rev.*, **136**, 1284–1304, doi:10.1175/2007MWR2245.1.
- Mei, W., S.-P. Xie, and M. Zhao, 2014: Variability of tropical cyclone track density in the North Atlantic: Observations and high-resolution simulations. *J. Climate*, **27**, 4797–4814, doi:10.1175/JCLI-D-13-00587.1.
- Murakami, H., and B. Wang, 2010: Future change of North Atlantic tropical cyclone tracks: Projection by a 20-km-mesh global atmospheric model. *J. Climate*, **23**, 2699–2721, doi:10.1175/2010JCLI3338.1.
- Oouchi, K., J. Yoshimura, H. Yoshimura, R. Mizuta, S. Kusunoki, and A. Noda, 2006: Tropical cyclone climatology in a global warming climate as simulated in a 20 km mesh global atmospheric model: Frequency and intensity analysis. *J. Meteor. Soc. Japan*, **84**, 259–276, doi:10.2151/jmsj.84.259.
- Patricola, C. M., R. Saravanan, and P. Chang, 2014: The impact of El Niño–Southern Oscillation and Atlantic meridional mode on seasonal Atlantic tropical cyclone activity. *J. Climate*, **27**, 5311–5328, doi:10.1175/JCLI-D-13-00687.1.
- Ramsay, H. A., S. J. Camargo, and D. Kim, 2012: Cluster analysis of tropical cyclone tracks in the Southern Hemisphere. *Climate Dyn.*, **39**, 897–917, doi:10.1007/s00382-011-1225-8.
- Rao, B. V. B., D. Hari Prasad, D. Srinivas, and Y. Anjaneyulu, 2010: Role of vertical resolution in numerical models towards the intensification, structure and track of tropical cyclones. *Mar. Geod.*, **33**, 338–355, doi:10.1080/01490419.2010.518066.
- Rayner, N. A., D. E. Parker, E. B. Horton, C. K. Folland, L. V. Alexander, D. P. Rowell, E. C. Kent, and A. Kaplan, 2003: Global analyses of SST, sea ice and night marine air temperature since the late nineteenth century. *J. Geophys. Res.*, **108**, 4407, doi:10.1029/2002JD002670.
- Reed, K. A., and C. Jablonowski, 2011a: Impact of physical parametrization on idealized tropical cyclones in the Community Atmosphere Model. *Geophys. Res. Lett.*, **38**, L048045, doi:10.1029/2010GL046297.
- , and —, 2011b: Assessing the uncertainty of tropical cyclone simulations in NCAR’s Community Atmosphere Model. *J. Adv. Model. Earth Syst.*, **3**, M08002, doi:10.1029/2011MS000076.
- , and —, 2012: Idealized tropical cyclone simulations of intermediate complexity: A test case for AGCMs. *J. Adv. Model. Earth Syst.*, **4**, M04001, doi:10.1029/2011MS000099.
- Rienecker, M. M., and Coauthors, 2008: The GEOS-5 Data Assimilation System—Documentation of versions 5.0.1, 5.1.0, and 5.2.0. NASA Global Modeling and Data Assimilation Tech. Rep. NASA/TM-2008-104606, Vol. 27, 118 pp.
- Roeckner, E., and Coauthors, 2003: The atmospheric general circulation model ECHAM5. Part I: Model description. MPI Rep. 349, 127 pp.
- Rotunno, R., Y. Chen, W. Wang, C. Davis, J. Dudhia, and C. L. Holland, 2009: Large-eddy simulation of an idealized tropical cyclone. *Bull. Amer. Meteor. Soc.*, **90**, 1783–1788, doi:10.1175/2009BAMS2884.1.
- Saha, S., and Coauthors, 2014: The NCEP Climate Forecast System version 2. *J. Climate*, **27**, 2185–2208, doi:10.1175/JCLI-D-12-00823.1.
- Schmidt, G. A., and Coauthors, 2014: Configuration and assessment of the GISS ModelE2 contributions to the CMIP5 archive. *J. Adv. Model. Earth Syst.*, **6**, 141–184, doi:10.1002/2013MS000265.
- Schubert, W. H., and J. J. Hack, 1983: Transformed Eliassen-balanced vortex model. *J. Atmos. Sci.*, **40**, 1571–1583, doi:10.1175/1520-0469(1983)040<1571:TEBVM>2.0.CO;2.
- Scoccimarro, E., and Coauthors, 2011: Effects of tropical cyclones on ocean heat transport in a high-resolution coupled general circulation model. *J. Climate*, **24**, 4368–4384, doi:10.1175/2011JCLI4104.1.

- , S. Gualdi, G. Villarini, G. A. Vecchi, M. Zhao, K. Walsh, and A. Navarra, 2014: Intense precipitation events associated with landfalling tropical cyclones in response to a warmer climate and increased CO₂. *J. Climate*, **27**, 4642–4654, doi:10.1175/JCLI-D-14-00065.1.
- Shaevitz, D. A., and Coauthors, 2015: Characteristics of tropical cyclones in high-resolution models of the present climate. *J. Adv. Model. Earth Syst.*, doi:10.1002/2014MS000372, in press.
- Skamarock, W. C., and Coauthors, 2008: A description of the Advanced Research WRF version 3. NCAR Tech. Note NCAR/TN-475+STR, 123 pp.
- Stocker, T. F., and Coauthors, Eds., 2014: *Climate Change 2013: The Physical Science Basis*. Cambridge University Press, 1535 pp.
- Strachan, J., P. L. Vidale, K. Hodges, M. Roberts, and M.-E. Demory, 2013: Investigating global tropical cyclone activity with a hierarchy of AGCMs: The role of model resolution. *J. Climate*, **26**, 133–152, doi:10.1175/JCLI-D-12-00012.1.
- Strazzo, S., J. B. Elsner, T. LaRow, D. Halperin, and M. Zhao, 2013: Observed versus GCM-generated local tropical cyclone frequency: Comparisons using a spatial lattice. *J. Climate*, **26**, 8257–8268, doi:10.1175/JCLI-D-12-00808.1.
- Sugi, M., A. Noda, and N. Sato, 2002: Influence of global warming on tropical cyclone climatology: An experiment with the JMA global model. *J. Meteor. Soc. Japan*, **80**, 249–272, doi:10.2151/jmsj.80.249.
- Villarini, G., and G. A. Vecchi, 2013: Projected increases in North Atlantic tropical cyclone intensity from CMIP5 models. *J. Climate*, **26**, 3231–3240, doi:10.1175/JCLI-D-12-00441.1.
- , D. A. Lavers, E. Scoccimarro, M. Zhao, M. F. Wehner, G. Vecchi, and T. Knutson, 2014: Sensitivity of tropical cyclone rainfall to idealized global scale forcings. *J. Climate*, **27**, 4622–4641, doi:10.1175/JCLI-D-13-00780.1.
- Vitart, F., D. Anderson, and T. Stockdale, 2003: Seasonal forecasting of tropical cyclone landfall over Mozambique. *J. Climate*, **16**, 3932–3945, doi:10.1175/1520-0442(2003)016<3932:SFOTCL>2.0.CO;2.
- Walsh, K., 1997: Objective detection of tropical cyclones in high-resolution analyses. *Mon. Wea. Rev.*, **125**, 1767–1779, doi:10.1175/1520-0493(1997)125<1767:ODOTCI>2.0.CO;2.
- , M. Fiorino, C. W. Landsea, and K. L. McInnes, 2007: Objectively determined resolution-dependent threshold criteria for the detection of tropical cyclones in climate models and reanalyses. *J. Climate*, **20**, 2307–2314, doi:10.1175/JCLI4074.1.
- , S. Lavender, H. Murakami, E. Scoccimarro, L.-P. Caron, and M. Ghantous, 2010: The Tropical Cyclone Climate Model Intercomparison Project. *Hurricanes and Climate Change*, Vol. 2, J. B. Elsner et al., Eds., Springer, 1–24.
- , —, E. Scoccimarro, and H. Murakami, 2013: Resolution dependence of tropical cyclone formation in CMIP3 and finer resolution models. *Climate Dyn.*, **40**, 585–599, doi:10.1007/s00382-012-1298-z.
- , and Coauthors, 2015: Hurricanes and climate: The U.S. CLIVAR working group on hurricanes. *Bull. Amer. Meteor. Soc.*, doi:10.1175/BAMS-D-13-00242.1, in press.
- Walters, D. N., and Coauthors, 2011: The Met Office Unified Model Global Atmosphere 3.0/3.1 and JULES Global Land 3.0/3.1 configurations. *Geosci. Model Dev.*, **4**, 919–941, doi:10.5194/gmd-4-919-2011.
- Wang, H., and Coauthors, 2014: How well do global climate models simulate the variability of Atlantic tropical cyclones associated with ENSO? *J. Climate*, **27**, 5673–5692, doi:10.1175/JCLI-D-13-00625.1.
- Wehner, M. F., and Coauthors, 2015: The effect of horizontal resolution on AMIP simulation quality in the Community Atmospheric Model, CAM5.1. *J. Model. Earth Syst.*, doi:10.1002/2013MS000276, in press.
- Yoshimura, J., and M. Sugi, 2005: Tropical cyclone climatology in a high-resolution AGCM—Impacts of SST warming and CO₂ increase. *SOLA*, **1**, 133–136, doi:10.2151/sola.2005-035.
- , —, and A. Noda, 2006: Influence of greenhouse warming on tropical cyclone frequency. *J. Meteor. Soc. Japan*, **84**, 405–428, doi:10.2151/jmsj.84.405.
- Zarzycki, C. M., and C. Jablonowski, 2014: A multidecadal simulation of Atlantic tropical cyclones using a variable-resolution global atmospheric general circulation model. *J. Adv. Model. Earth Syst.*, **6**, 805–828, doi:10.1002/2014MS000352.
- Zhang, D. L., and H. Wang, 2003: Dependence of hurricane intensity and structures on vertical resolution and time-step size. *Adv. Atmos. Sci.*, **20**, 711–725, doi:10.1007/BF02915397.
- Zhao, M., and I. M. Held, 2010: An analysis of the effect of global warming on the intensity of Atlantic hurricanes using a GCM with statistical refinement. *J. Climate*, **23**, 6382–6393, doi:10.1175/2010JCLI3837.1.
- , and —, 2012: TC-permitting GCM simulations of hurricane frequency response to sea surface temperature anomalies projected for the late-twenty-first century. *J. Climate*, **25**, 2995–3009, doi:10.1175/JCLI-D-11-00313.1.
- , —, S.-J. Lin, and G. A. Vecchi, 2009: Simulations of global hurricane climatology, interannual variability, and response to global warming using a 50-km resolution GCM. *J. Climate*, **22**, 6653–6678, doi:10.1175/2009JCLI3049.1.
- , —, and —, 2012: Some counterintuitive dependencies of tropical cyclone frequency on parameters in a GCM. *J. Atmos. Sci.*, **69**, 2272–2283, doi:10.1175/JAS-D-11-0238.1.
- , and Coauthors, 2013: Robust direct effect of increasing atmospheric CO₂ concentration on global tropical cyclone frequency: A multi-model inter-comparison. *U.S. CLIVAR Variations*, Vol. 11, No. 3, U.S. Climate Variability and Predictability Program, Washington, D.C., 17–23.